

---

# POWERING UP ZEROTH-ORDER TRAINING VIA SUBSPACE GRADIENT ORTHOGONALIZATION

---

A PREPRINT

**Yicheng Lang<sup>1</sup> Changsheng Wang<sup>1</sup> Yihua Zhang<sup>1</sup> Mingyi Hong<sup>2</sup>**  
**Zheng Zhang<sup>3</sup> Wotao Yin<sup>4</sup> Sijia Liu<sup>1,5</sup>**

<sup>1</sup>Michigan State University <sup>2</sup>University of Minnesota <sup>3</sup>University of California, Santa Barbara

<sup>4</sup>DAMO Academy, Alibaba Group US <sup>5</sup>IBM Research, USA

## ABSTRACT

Zeroth-order (ZO) optimization provides a gradient-free alternative to first-order (FO) methods by estimating gradients via finite differences of function evaluations, and has recently emerged as a memory-efficient paradigm for fine-tuning large-scale models by avoiding backpropagation. However, ZO optimization has a fundamental tension between accuracy and query efficiency. In this work, we show that ZO optimization can be substantially improved by unifying two complementary principles: (i) a projection-based subspace view that reduces gradient estimation variance by exploiting the intrinsic low-rank structure of model updates, and (ii) Muon-style spectral optimization that applies gradient orthogonalization to extract informative spectral structure from noisy ZO gradients. These findings form a unified framework of subspace gradient orthogonalization, which we instantiate in a new method, **ZO-Muon**, admitting a natural interpretation as a low-rank Muon optimizer in the ZO setting. Extensive experiments on large language models (LLMs) and vision transformers (ViTs) demonstrate that ZO-Muon significantly accelerates convergence and achieves a win-win improvement in accuracy and query/runtime efficiency. Notably, compared to the popular MeZO baseline, ZO-Muon requires only 24.7% of the queries to reach the same SST-2 performance for LLM fine-tuning, and improves accuracy by 25.1% on ViT-B fine-tuning on CIFAR-100. Code is available at <https://github.com/OPTML-Group/ZO-Muon>.

## 1 Introduction

Training deep models such as large language models (LLMs) (Achiam et al., 2023; Zhang et al., 2022a; Touvron et al., 2023) relies on backpropagation (BP) to compute first-order (FO) gradients for optimization (Amari, 1993; Kingma, 2014). However, as model sizes scale, the GPU memory cost of BP grows substantially (Chen et al., 2025a). This motivates a fundamental question with practical impact: Can deep models be trained in a *gradient-free* manner without relying on BP? Toward this end, zeroth-order (ZO) optimization (Liu et al., 2020a; Duchi et al., 2015; Nesterov and Spokoiny, 2017) offers a theoretically grounded alternative to FO optimization by estimating gradients via finite differences of function values using only forward passes of the model, thereby substantially reducing the memory footprint during training (Malladi et al., 2023; Zhang et al., 2024; Tan et al., 2025a; Liu et al., 2025a). Although ZO optimization also arises in black-box or gray-box application settings (Chen et al., 2017; Ilyas et al., 2018; Zhao et al., 2019; Chen et al., 2023) (where FO gradients are infeasible or inaccessible), *memory-efficient fine-tuning of large models* has recently become one of its most impactful and arguably primary applications, as first proposed in (Malladi et al., 2023) and a focus of this work.

Despite the promise of ZO optimization, achieving convergence and accuracy comparable to FO optimization remains highly nontrivial. A key challenge of ZO optimization is the high variance of query-based gradient estimation, which becomes increasingly severe as the problem dimension grows (Duchi et al., 2015; Nesterov and Spokoiny, 2017; Liu et al., 2018a,b; Chen et al., 2023). Therefore, to reduce the variance of ZO gradient estimation, existing work has focused on designing improved gradient estimators. Examples include preconditioning the estimator with Hessian information (Zhao et al., 2025b,a), optimizing perturbation directions before computing directional derivatives (Ma and Huang, 2025), and imposing structural priors such as sparsity (Guo et al., 2024; Liu et al., 2025a) or low-rankness (Chen et al., 2025b; Yu et al., 2025) in the gradient estimation. However, these estimator-centric designs still primarily

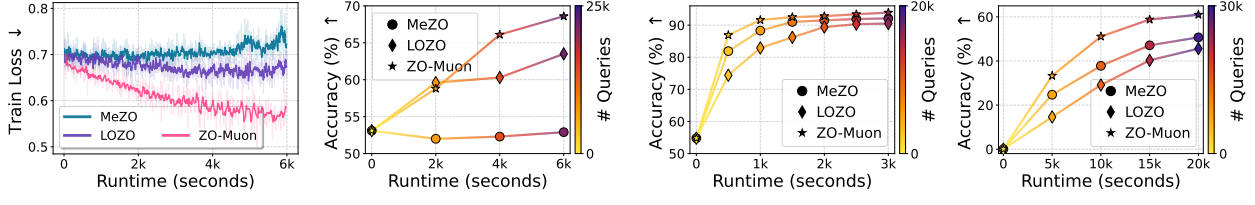
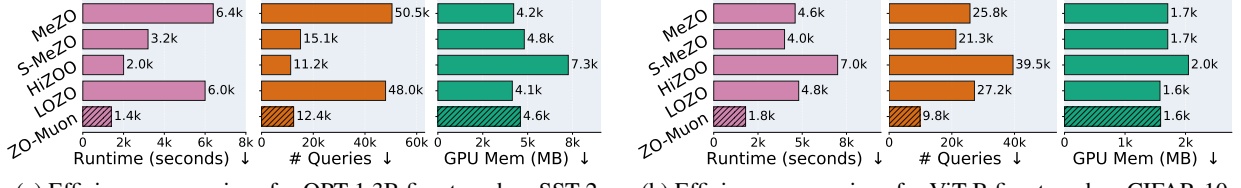
(a) *LLM fine-tuning*: OPT-1.3B on RTE(b) *ViT fine-tuning*: ViT-B on CIFAR-10 (left) & 100 (right)

Figure 1: ZO-Muon achieves faster convergence and better fine-tuning accuracy than the SOTA ZO baselines MeZO (Malladi et al., 2023) and LOZO (Chen et al., 2025b) against runtime. (a) OPT-1.3B fine-tuned on the RTE task: training loss (left) and test accuracy (right) versus runtime, with the cumulative query count indicated by the color bar in the right subplot. (b) ViT-B fine-tuned on CIFAR-10 (left) and CIFAR-100 (right), shown in the same format as in (a, right).



(a) Efficiency comparison for OPT-1.3B fine-tuned on SST-2

(b) Efficiency comparison for ViT-B fine-tuned on CIFAR-10

Figure 2: ZO-Muon yields lower runtime and fewer function queries than all baselines (under comparable GPU memory usage), when reaching the target fine-tuning accuracies: (a) 0.90 on SST-2 and (b) 0.93 on CIFAR-10. Baselines include MeZO (Malladi et al., 2023), SparseMeZO (S-MeZO) (Liu et al., 2025a), HiZOO (Zhao et al., 2025a), and LOZO (Chen et al., 2025b).

operate in the original parameter space of the model, which limits the extent of variance reduction. As a result, the performance gap between ZO and FO still remains for deep model training.

Another principled approach to reducing variance in ZO optimization is to use multiple queries (at the cost of increased query complexity) to average out estimation noise. However, a linear increase in the number of queries (or runtime) yields only a *sub-linear* improvement in performance (and may even lead to a multi-query paradox with no improvement) (Lin et al., 2025), making it challenging to strike a favorable *accuracy-efficiency trade-off*. For example, FZOO (Dang et al., 2025) requires a substantial number of queries to estimate the variance of function evaluations for gradient normalization. Similarly, SVRG-based ZO methods (Liu et al., 2018b; Ji et al., 2019) also require an excessive number of queries to construct error-correction terms for determining descent directions from estimated gradients. ZO-Align (Lin et al., 2025) leverages projection alignment across multiple queries, but is difficult to scale because it must store multiple ZO gradients in large matrices. MUZO (Peng et al., 2025) takes not only multiple queries but also the more complex Adam optimizer in ZO optimization, which incurs additional memory overhead.

As mentioned above, although ZO model training has made substantial recent progress, its core bottlenecks, limited accuracy due to high variance and a poor accuracy-efficiency trade-off, remain unresolved. Thus, we ask:

**(Q)** *Can we advance ZO optimization for model training to achieve a win-win in both accuracy and efficiency?*

To address **(Q)**, we propose a novel *subspace gradient orthogonalization* viewpoint to revisit and redesign ZO optimization. This framework consists of two key components: *projection-based subspace ZO optimization* and *gradient-orthogonalized spectral optimization*. The former reduces the variance of ZO gradient estimation by projecting the original full-space problem into a lower-dimensional subspace. The latter further improves optimization accuracy by leveraging gradient orthogonalization in the recent Muon optimizer (Jordan et al., 2024; Liu et al., 2025b), which can extract meaningful descent directions from noisy ZO gradient estimates rather than directly using their entry-wise values. We term the proposed subspace gradient orthogonalization-based ZO optimization approach “**ZO-Muon**” to echo its connection to Muon. As shown in **Fig. 1** and **Fig. 2**, ZO-Muon consistently outperforms a range of state-of-the-art (SOTA) baselines in both convergence speed and accuracy. Moreover, these performance gains do not incur additional query cost under the same runtime budget, indicating improved efficiency in both runtime and query usage across LLM and ViT fine-tuning tasks. This achieves the desired win-win outcome posed in **(Q)**.

We summarize our main **contributions** as follows.

① (Formulation) We revisit ZO optimization from a projection-based perspective and propose a *subspace randomized gradient estimator* (Subspace RGE), which substantially reduces the variance of gradient estimation by operating in a low-dimensional subspace.

② (Algorithm) We show that Muon’s *gradient orthogonalization* provides complementary gains to Subspace RGE, yielding a more stable and faster multi-query ZO optimization algorithm, termed **ZO-Muon**.

③ (Experiment) Compared with the stateful baselines including MeZO (Malladi et al., 2023), LOZO (Chen et al., 2025b), SparseMeZO (Liu et al., 2025a), HiZOO (Zhao et al., 2025a), and SubZero (Yu et al., 2025), ZO-Muon consistently delivers superior accuracy and efficiency; see Figs. 1–2 for representative results.

## 2 Related Work

**ZO optimization and applications in deep models.** ZO optimization (Ghadimi and Lan, 2013; Duchi et al., 2015; Nesterov and Spokoiny, 2017; Balasubramanian and Ghadimi, 2022; Liu et al., 2020a) estimates gradients via finite differences of function values without computing FO derivatives. As detailed in Sec. 1 and thus omitted here for brevity, a large body of foundational work on ZO optimization has focused on reducing estimation variance to improve accuracy and the trade-off with query efficiency. In contrast, in this work we show that our approach achieves a *win-win* improvement in both accuracy and efficiency for the first time. Empirically, the success of ZO methods has been initially demonstrated in solving small-scale problems, such as input-level black-box adversarial attack and defense (Chen et al., 2017; Tu et al., 2019; Chen et al., 2019; Cheng et al., 2019; Ilyas et al., 2018; Liu et al., 2020b; Zhang et al., 2022b), input-level prompt design for foundation models (Sun et al., 2022; Hu et al., 2024; Zhang et al., 2025a), and resource-limited on-device learning (Gu et al., 2021; Zhang et al., 2025b; Tan et al., 2025b). More recently, the application of ZO optimization has shifted toward larger-scale deep model training, including black-box or non-differentiable-component-involved training from scratch (Chen et al., 2023) and memory-efficient fine-tuning (Zhang et al., 2024; Malladi et al., 2023; Tan et al., 2025a; Liu et al., 2025a).

**Subspace optimization for efficient training.** Motivated by the observation that weights or gradients in deep model training often exhibit low-rank structure (Kaushik et al., 2025; Aghajanyan et al., 2021; Hu et al., 2022; Zhao et al., 2024; Hao et al., 2024), a growing body of work has explored training in low-dimensional subspaces to improve memory efficiency. LoRA-style methods (Hu et al., 2022; Dettmers et al., 2023; Wang et al., 2025; Lion et al., 2025) directly constrain trainable parameters to low-rank matrices, but can be less effective in some settings due to the limited expressiveness of low-rank parameterizations (Hao et al., 2024) and insufficient directional diversity (Lion et al., 2025). Another line of work uses projection matrices to project gradients into low-dimensional subspaces, thereby reducing the memory footprint of optimizer states for memory-efficient fine-tuning (Zhao et al., 2024; He et al., 2024; Liang et al., 2024; Zhang et al., 2025c; Refael et al., 2025a). Subspace perspectives have also been explored in ZO optimization. LOZO (Chen et al., 2025b) adopts two low-dimensional Gaussian matrices for perturbation and model updates, while SubZero (Yu et al., 2025) leverages two column-orthonormal random matrices to sketch FO gradients and then estimate them in a much lower-dimensional space. In addition, (Kozak et al., 2023; Nozawa et al., 2025) provide theoretical formulations of ZO methods from a subspace optimization perspective, but do not consider practical large-scale model fine-tuning. In contrast, we propose a subspace projection-based view to revisit and redesign ZO optimization, and reveal a mutually beneficial synergy between subspace ZO and Muon-style gradient orthogonalization.

**Emerging gradient-orthogonalized methods for deep model training.** Recent years have witnessed growing interest in *gradient-orthogonalized* optimization methods for training large-scale deep models, particularly foundation models, driven by the need to exploit the matrix-structured and spectral properties of gradients that are poorly captured by conventional vector-based optimizers. The Muon optimizer (Jordan et al., 2024) and its subsequent variants (Liu et al., 2025b; Ma et al., 2025; Riabinin et al., 2025; Khaled et al., 2025; He et al., 2025; Ahn et al., 2025; Amsel et al., 2025) embody this shift by performing *gradient orthogonalization* (GO), which projects gradient updates onto a spectrally constrained set via matrix whitening and can be interpreted as a steepest-descent step under a spectral-norm constraint (Bernstein and Newhouse, 2024). This spectral treatment leads to faster convergence and reduced optimizer-state memory compared to Adam, enabling Muon to scale to foundation-model training, most notably in Moonlight (Liu et al., 2025b), a 3B/16B Mixture-of-Experts (MoE) model.

Despite this progress, GO has remained largely confined to *FO pre-training*, and extending it to ZO settings is nontrivial due to the lower quality of ZO gradient estimates. JAGUAR-Muon (Petrov et al., 2025) attempts to apply GO to full-space ZO momentum, but incurs additional memory and runtime overhead over MeZO (Malladi et al., 2023) and shows very limited performance gain. This is likely because applying GO to noisy, high-dimensional ZO estimates amplifies non-informative spectral components, a limitation also confirmed by our experiments. By contrast, we show that GO becomes effective for ZO optimization *only when coupled with a subspace formulation*, which we term *subspace gradient orthogonalization*.

## 3 Rethinking ZO Optimization: From Full Space to A Projected Subspace View

In this section, we first introduce the standard ZO optimization formulation, whose core algorithmic component is a query-based ZO gradient estimator built from finite differences of function values. We then develop a new projection-based subspace perspective, from which we derive a subspace ZO gradient estimator and motivate its effectiveness for improving ZO accuracy and query efficiency.

**Standard ZO optimization in the full space.** Consider a standard minimization problem with variable  $\mathbf{X} \in \mathbb{R}^{m \times n}$ :

$$\underset{\mathbf{X}}{\text{minimize}} \quad f(\mathbf{X}), \quad (1)$$

where, instead of vectorizing the variable  $\mathbf{X}$  (*e.g.*, model weights or weight perturbations to a pre-trained model for fine-tuning), we use its matrix form for notational consistency throughout the paper. Here,  $f$  denotes the objective function (*e.g.*, the fine-tuning loss for a downstream task).

To solve problem (1), the standard ZO optimization approach replaces the gradient used in FO methods with a query-based ZO gradient estimator constructed from finite differences of function values (Liu et al., 2020a). A standard choice is the *randomized gradient estimator (RGE)* (Nesterov and Spokoiny, 2017), whose effectiveness for memory-efficient LLM fine-tuning has been demonstrated by MeZO (Malladi et al., 2023), which is built upon ZO-SGD. A *generic form of the RGE* (Duchi et al., 2015) is given by

$$\hat{\nabla}_{\mathbf{X}} f(\mathbf{X}) = \frac{1}{N_q} \sum_{i=1}^{N_q} \frac{f(\mathbf{X} + \mu \Psi_i) - f(\mathbf{X})}{\mu} \Psi_i, \quad (2)$$

where  $\hat{\nabla}_{\mathbf{X}} f(\mathbf{X})$  denotes the estimated gradient of  $f$  with respect to (w.r.t.)  $\mathbf{X}$ ,  $N_q$  denotes the number of queries,  $\Psi_i \in \mathbb{R}^{m \times n}$  is a random perturbation matrix applied to the optimization variable  $\mathbf{X}$  whose entries are independently drawn from the standard Gaussian distribution, and  $\mu > 0$  is a small smoothing (perturbation) parameter. As shown in (2), the RGE is constructed using the *forward-difference* approximation of function values for each query. An alternative variant adopts the *central-difference* scheme,  $\frac{f(\mathbf{X} + \mu \Psi) - f(\mathbf{X} - \mu \Psi)}{2\mu} \Psi$ , which is used by MeZO (Malladi et al., 2023). In this work, we prefer the forward-difference estimator when  $N_q > 1$  due to its lower query complexity: the RGE in (2) requires only  $(N_q + 1)$  function queries, compared to  $2N_q$  queries for the central-difference scheme. When  $N_q = 1$ , the query complexity of the two schemes is the same; therefore, we use the central-difference estimator.

The RGE (2) provides an unbiased estimator of the gradient of a smoothed version of the original objective, *i.e.*,  $\mathbb{E}_{\Psi}[f(\mathbf{X} + \mu \Psi)]$ , and its estimation variance scales as  $O(mn/N_q)$  (Liu et al., 2020a). Consequently, a fundamental limitation of RGE is its high gradient estimation variance, which scales proportionally with the problem dimension and can become prohibitively large for training large-scale models. In theory, mitigating this variance requires using a large number of queries  $N_q$ , leading to an unfavorable variance-query trade-off.

**Subspace ZO optimization: A projection-based view.** A growing body of evidence suggests that, in deep model training, the weights and their gradients evolve within a much lower-dimensional subspace (Aghajanyan et al., 2021; Hu et al., 2022; Zhao et al., 2024; Kaushik et al., 2025).

Therefore, it is natural to ask *whether one can transition ZO optimization from the full space to a subspace*, where the RGE can be obtained with significantly reduced variance due to the reduced effective problem dimension.

Motivated by the above, we propose to approximate the original problem (1) via a projected variant, under the implicit assumption that the optimization variable  $\mathbf{X}$  admits a low-dimensional representation after projection. To be concrete, let  $\mathbf{P} \in \mathbb{R}^{m \times r}$  denote a projection matrix whose  $r$  columns (with  $r \ll \min\{m, n\}$ ) are *orthonormal*, *i.e.*,  $\mathbf{P}^T \mathbf{P} = \mathbf{I}_r$ , where  $\mathbf{I}_r \in \mathbb{R}^{r \times r}$  denotes the identity matrix. We then represent the original variable  $\mathbf{X}$  using a lower-dimensional representation  $\mathbf{Z} \in \mathbb{R}^{r \times n}$  over the subspace spanned by the columns of  $\mathbf{P}$ , yielding the approximation  $\mathbf{X} \approx \mathbf{PZ}$ . We choose  $\mathbf{P}$  to be a *random column-orthonormal* projection matrix (that can be readily obtained via QR decomposition of a random Gaussian matrix) and approximate (1) as:

$$\underset{\mathbf{Z} \in \mathbb{R}^{r \times n}}{\text{minimize}} \quad \mathbb{E}_{\mathbf{P}}[f(\mathbf{PZ})]. \quad (3)$$

We will show that the above provides a  $\mathbf{P}$ -projected view of (1) that is sufficient to guide effective ZO optimization.

To further understand the relationship between the original problem (1) and its projected approximation (3), we examine the FO (stochastic) gradient of the latter w.r.t. the lower-dimensional variable  $\mathbf{Z}$ . This yields

$$\underbrace{\nabla_{\mathbf{Z}} f(\mathbf{PZ})}_{\textcircled{1} \text{ gradient in } \mathbf{Z} \text{ space}} = \mathbf{P}^T \nabla_{\mathbf{X}} f(\mathbf{X}), \quad \underbrace{\mathbf{P} \nabla_{\mathbf{Z}} f(\mathbf{PZ})}_{\textcircled{2} \text{ gradient lifting back to } \mathbf{X} \text{ space}} = \mathbf{P} \mathbf{P}^T \nabla_{\mathbf{X}} f(\mathbf{X}). \quad (4)$$

Here, the transition from  $\textcircled{1}$  to  $\textcircled{2}$  indicates that the subspace gradient  $\nabla_{\mathbf{Z}} f(\mathbf{PZ})$ , when lifted back to the full space via the same projection matrix  $\mathbf{P}$ , yields a projected full-space gradient  $\mathbf{P} \mathbf{P}^T \nabla_{\mathbf{X}} f(\mathbf{X})$ . Defining  $\hat{\mathbf{P}} := \mathbf{P} \mathbf{P}^T \in \mathbb{R}^{m \times m}$ , we note that  $\hat{\mathbf{P}}$  is a projection matrix that maps any vector onto the subspace spanned by the columns of  $\mathbf{P}$  and satisfies the idempotence property  $\hat{\mathbf{P}}^2 = \hat{\mathbf{P}}$  (due to  $\mathbf{P}^T \mathbf{P} = \mathbf{I}_r$ ).

The key implications of (4) for ZO optimization are as follows. Under the projected formulation (3), we can apply the RGE in (2) directly in the reduced  $\mathbf{Z}$ -space to obtain a dimension-reduced (and hence variance-reduced) ZO gradient

estimate  $\hat{\nabla}_{\mathbf{Z}} f(\mathbf{PZ})$ , corresponding to the ZO realization of step ① in (4). This is given by

$$\hat{\nabla}_{\mathbf{Z}} f(\mathbf{PZ}) = \frac{1}{N_q} \sum_{i=1}^{N_q} \frac{f(\mathbf{X} + \mu \mathbf{P} \Psi_i) - f(\mathbf{X})}{\mu} \Psi_i, \quad (5)$$

where in contrast to the standard RGE in (2), the perturbation  $\Psi_i \in \mathbb{R}^{r \times n}$  is applied to the lower-dimensional subspace variable  $\mathbf{Z}$ , and we write the function value  $f(\mathbf{PZ})$  using the exact correspondence between  $\mathbf{PZ}$  and  $\mathbf{X}$ .

The advantage of the ZO gradient estimator in (5) w.r.t.  $\mathbf{Z}$  lies in its reduced estimation variance. Next, to obtain a full-space gradient estimate, we leverage step ② in (4) to lift the subspace ZO gradient in (5) back to the original space, yielding a ZO gradient estimate w.r.t.  $\mathbf{X}$ , which we term **Subspace RGE** due to its reliance on (5):

$$\begin{aligned} \hat{\nabla}_{\mathbf{X}} f(\mathbf{X}) &\approx \mathbf{P} \hat{\nabla}_{\mathbf{Z}} f(\mathbf{PZ}) \\ &= \mathbf{P} \left[ \frac{1}{N_q} \sum_{i=1}^{N_q} \frac{f(\mathbf{X} + \mu \mathbf{P} \Psi_i) - f(\mathbf{X})}{\mu} \Psi_i \right] \\ &= \frac{1}{N_q} \sum_{i=1}^{N_q} \frac{f(\mathbf{X} + \mu \mathbf{P} \Psi_i) - f(\mathbf{X})}{\mu} \mathbf{P} \Psi_i. \end{aligned} \quad (6)$$

As indicated by (4), the Subspace RGE (6) serves as the ZO counterpart of the projected FO gradient  $\mathbf{P} \mathbf{P}^\top \nabla_{\mathbf{X}} f(\mathbf{X})$ , rather than of the full gradient. Although this introduces an estimation bias at first glance, in practice it can actually lead to improved ZO optimization performance due to two key factors: (i) the variance reduction benefit enjoyed by (5), and (ii) the intrinsic subspace structure of gradients during model training which makes subspace projection effectively lossless, as will be validated below.

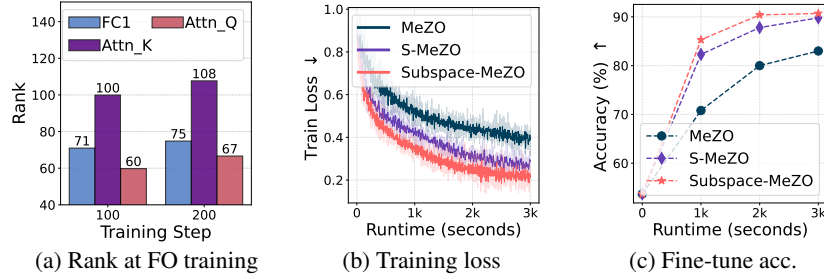


Figure 3: The necessity and advantages of Subspace RGE, illustrated by fine-tuning OPT-1.3B on SST-2: (a) The low-rank structure of model components during FO training with Adam across steps; (b) Performance comparison of Subspace RGE-based MeZO (i.e., Subspace-MeZO) with the SOTA baselines SparseMeZO (i.e., S-MeZO) and MeZO; And (c) accuracy vs. runtime.

**Fig. 3** provides a motivating example based on fine-tuning OPT-1.3B on the SST-2 task, which illustrates the above rationale for using the Subspace RGE in (6) instead of the vanilla RGE in (2). Fig. 3(a) shows that the FO gradients during Adam-based training exhibit a pronounced low-rank structure, where the effective rank is measured by the number of top singular values required to capture 99.99% of the spectral energy (see **Appendix A** for details). In addition, we refer to the integration of Subspace RGE (at  $N_q = 1$ ) into MeZO as **Subspace-MeZO**, and include MeZO (Malladi et al., 2023) and SparseMeZO (Liu et al., 2025a) as baselines; see **Sec. 5.1** for experimental setups. As shown, Subspace-MeZO achieves both faster convergence (Fig. 3(b)) and better accuracy (Fig. 3(c)).

**Comparison with prior work: A closer look at Subspace RGE.** The last equality in (6) suggests that Subspace RGE can be implemented in the same form as the standard RGE (2), but using  $\mathbf{P} \Psi$  as the effective perturbation which admits a low-rank factorization into  $\mathbf{P} \in \mathbb{R}^{m \times r}$  and  $\Psi \in \mathbb{R}^{r \times n}$  since  $r \ll \min\{m, n\}$ . Here, we omit the query index of  $\Psi$  for brevity. This perspective connects the proposed Subspace RGE to the existing low-rank ZO optimization approach, **LOZO** (Chen et al., 2025b). We provide a detailed comparison between our proposal and LOZO below.

LOZO (Chen et al., 2025b) incorporates low-rank perturbations into the (central-difference) RGE in (2), yielding the *low-rank gradient estimator* (LGE).

$$\hat{\nabla}_{\mathbf{X}} f(\mathbf{X}) = \frac{f(\mathbf{X} + \mu \mathbf{AB}) - f(\mathbf{X} - \mu \mathbf{AB})}{2\mu} \mathbf{AB}, \quad (7)$$

where  $\mathbf{A} \in \mathbb{R}^{m \times r}$  and  $\mathbf{B} \in \mathbb{R}^{r \times n}$  are two random matrices from standard Gaussian distributions with  $r \ll \min\{m, n\}$ . The overall perturbation  $\mathbf{AB}$  thus gives a low-rank, factorized approximation of the full-space perturbation  $\Psi$  in (2).

A comparison between the LGE in (7) and the proposed Subspace RGE in (6) shows that the two estimators take essentially the same form, up to a swap between the left perturbation matrices  $\mathbf{A}$  and  $\mathbf{P}$ , and between the right perturbation matrices  $\mathbf{B}$  and  $\Psi$ . However, beyond this formal similarity, there exists a *key difference* in the choice of the (left) perturbation matrix: Subspace RGE enforces  $\mathbf{P}$  to be *column-orthonormal*, whereas LGE imposes no such constraint on  $\mathbf{A}$ . This distinction is critical because  $\mathbf{P}$  in Subspace RGE admits a natural interpretation as a subspace projector, which is precisely why it estimates the projected gradient  $\hat{\mathbf{P}}\nabla_{\mathbf{X}}f(\mathbf{X})$  in step ② of (4), where  $\hat{\mathbf{P}} = \mathbf{P}\mathbf{P}^\top$ . Recall that  $\hat{\mathbf{P}}$  is a projection matrix satisfying the idempotence property, and it is easy to verify that  $(\mathbf{I} - \hat{\mathbf{P}})$  is also a projection matrix onto the subspace orthogonal to the column space of  $\mathbf{P}$ . The above indicates that the full gradient naturally admits the decomposition  $\nabla_{\mathbf{X}}f(\mathbf{X}) = \hat{\mathbf{P}}\nabla_{\mathbf{X}}f(\mathbf{X}) + (\mathbf{I} - \hat{\mathbf{P}})\nabla_{\mathbf{X}}f(\mathbf{X})$ , where  $(\mathbf{I} - \hat{\mathbf{P}})$  is the complementary projection. Therefore, the use of a column-orthonormal matrix  $\mathbf{P}$  in Subspace RGE endows the ZO method with a clear geometric interpretation about the FO gradient component it aims to estimate. By contrast, LOZO does not admit such an interpretation.

In addition to LOZO, SubZero (Yu et al., 2025) also develops a low-rank perturbation-based RGE similar to (7). Although, like us, SubZero considers column-orthonormal projections motivated by subspace optimization (Nozawa et al., 2025; Kozak et al., 2023), its use of projection is conceptually different from our viewpoint. In our framework, as formalized by steps ①–② and the derivation of (6), we treat subspace optimization as an explicit intermediate step: we first perform RGE in a reduced subspace and then lift the resulting gradient estimate back to the full space to solve the original ZO problem. This positioning is the key distinction between our work and prior approaches with similar algebraic forms. Furthermore, SubZero adopts two projection matrices, whose generation via QR decomposition could incur non-negligible runtime overhead, making such double-projection schemes less computationally efficient.

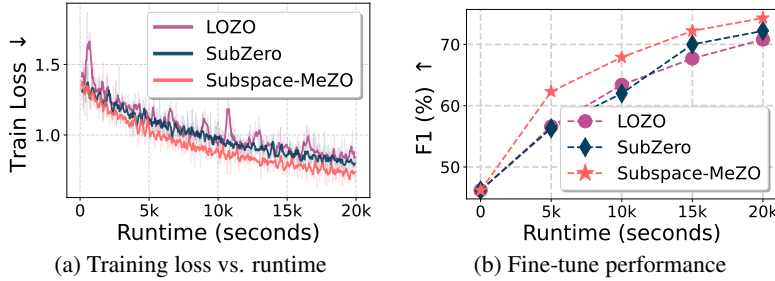


Figure 4: Training (a) and testing (b) performance comparison of the proposed Subspace RGE-based MeZO (i.e., Subspace-MeZO) with existing low-rank perturbation-based ZO baselines, LOZO (Chen et al., 2025b) and SubZero (Yu et al., 2025), for fine-tuning OPT-13B on SQuAD whose performance is measured by F1 (%).

In **Fig. 4**, we validate the advantage of the proposed subspace RGE within the Subspace-MeZO framework when fine-tuning OPT-13B on the SQuAD task. As shown, even when compared against LOZO and SubZero (in addition to MeZO and S-MeZO in Fig. 3), Subspace-MeZO achieves the fastest convergence (Fig. 4(a)) and the best fine-tuning performance (Fig. 4(b)) under the same runtime budget.

## 4 ZO-Muon: Boosting Subspace ZO via Gradient Orthogonalization

In this section, we show that *gradient orthogonalization* (GO), the core ingredient underlying the recently popular optimizer Muon (Jordan et al., 2024; Liu et al., 2025b), can be used to further boost the subspace ZO method in Sec. 3.

**Gradient orthogonalization in Muon: From FO to ZO, with insights from the failure of ZO-Muon-V0.** Before introducing ZO-Muon, we briefly recall the key idea behind FO Muon. Muon can be interpreted as a steepest-descent method under a spectral-norm constraint (Bernstein and Newhouse, 2024), or more broadly as a spectral optimization method that exploits the *matrix-level spectral structure* of descent directions rather than their *entry-wise* information.

Concretely, given the iterate  $\mathbf{X}_t$  of the optimization variable  $\mathbf{X}$  at iteration  $t$  and the learning rate  $\eta_t$ , the **basic Muon** (without momentum) takes the form (Jordan et al., 2024):

$$\mathbf{X}_{t+1} = \mathbf{X}_t - \eta_t \text{msign}(\mathbf{G}_t), \quad (8)$$

where  $\mathbf{G}_t$  denotes the (stochastic) gradient at iteration  $t$ , and  $\text{msign}(\cdot)$  denotes the matrix sign function, also known as matrix whitening transformation. The quantity  $\text{msign}(\mathbf{G}_t)$  can be interpreted as the descent direction obtained by projecting  $\mathbf{G}_t$  onto the spectral-norm unit ball (Khaled et al., 2025), which admits the closed-form expression:

$$\text{msign}(\mathbf{G}) = \mathbf{G}(\mathbf{G}^\top \mathbf{G})^{-\frac{1}{2}} = \mathbf{U} \text{sign}(\Sigma) \mathbf{V}^\top = \mathbf{U}_{[:,k]} \mathbf{V}_{[:,k]}^\top, \quad (9)$$

where  $\mathbf{G} = \mathbf{U}\Sigma\mathbf{V}^\top$  is the singular value decomposition (SVD) of  $\mathbf{G}$ , and  $\text{sign}(\cdot)$  denotes the (entry-wise) sign function, returning 1 for non-zero (positive) singular values and 0 otherwise. Moreover,  $\mathbf{U}_{[:,k]} \in \mathbb{R}^{m \times k}$  and  $\mathbf{V}_{[:,k]} \in \mathbb{R}^{n \times k}$  denote the submatrices of  $\mathbf{U}$  and  $\mathbf{V}$  consisting of their first  $k$  columns, respectively, where  $k$  is the *rank* of  $\mathbf{G}$ .

As shown in (9), the `mSIGN` operation plays the role of GO by equalizing all active singular directions and producing a spectrally isotropic update. This leads to the key benefit in Muon, which enables the model update to fully explore and exploit the spectral descent directions. In addition, Muon provides an efficient numerical approximation of `mSIGN` via Newton–Schulz (NS) iterations (Bernstein and Newhouse, 2024), avoiding the need to compute a full SVD.

Inspired by Muon’s spectral advantage, one may naturally ask whether exploiting such spectral information in the ZO gradient estimator can also bring similar benefits as in FO optimization. Accordingly, by replacing  $\mathbf{G}_t$  with its standard RGE counterpart in (2), we obtain a vanilla ZO-Muon variant, which we denote as **ZO-Muon-V0**, *i.e.*, applying GO directly to MeZO.

However, we find that ZO-Muon-V0 does *not* provide additional benefits over the GO-*absent* baseline, MeZO. As shown in Fig. 5, when fine-tuning OPT models on SST-2, ZO-Muon-V0 *underperforms* MeZO in both accuracy and runtime efficiency under the same query budget. This *accuracy* underperformance is likely because directly applying GO to noisy ZO gradient estimates amplifies spurious directions during matrix whitening, thereby degrading optimization performance. From a *runtime* perspective, performing the NS iterations for GO also introduces additional computational overhead compared to MeZO, *i.e.*, RGE-based ZO-SGD. In addition to ZO-Muon-V0, we also evaluate the ineffectiveness of JAGUAR-Muon (Petrov et al., 2025), another direct attempt to integrate Muon into ZO optimization; see Fig. A1 in Appendix B.

**ZO-Muon: How and why.** As motivated above, it is *nontrivial* to effectively leverage Muon’s spectral advantages in the ZO setting. In what follows, we show that the *subspace ZO* formulation in Sec. 3 is more suitable for integration with Muon. Our rationale is that Subspace RGE (5) induces a *low-rank* structure by estimating gradients in a low-dimensional subspace. When combined with GO, this effectively acts as a low-rank spectral filter that suppresses non-informative noise in the RGE. From an efficiency standpoint, the cost of the `mSIGN` operation in (9) scales with the matrix rank (He et al., 2025), so integrating GO with subspace ZO also improves computational efficiency. As confirmed by ZO-Muon in Fig. 5, *an accuracy-efficiency win-win emerges when GO meets subspace ZO*.

We next formally develop ZO-Muon. Recalling the projection-based view used to derive Subspace RGE in (6) from (4), we can integrate GO (*i.e.*, the `mSIGN` operation) with the subspace RGE in (5) on the lower-dimensional variable  $\mathbf{Z}$ , and then lift the resulting gradient-orthogonalized RGE back to the full space w.r.t. the original variable  $\mathbf{X}$ . This leads to **ZO-Muon** that modifies the Muon (8) to

$$\mathbf{O}_t = \mathbf{P} \text{msign} \left( \underbrace{\frac{1}{N_q} \sum_{i=1}^{N_q} \frac{f(\mathbf{X}_t + \mu \mathbf{P} \mathbf{\Psi}_i) - f(\mathbf{X}_t)}{\mu} \mathbf{\Psi}_i}_{\text{RGE } \hat{\nabla}_{\mathbf{Z}} f \text{ within subspace in (5), like step ① in (4)}} \right) \quad (10)$$

$$\mathbf{X}_{t+1} = \mathbf{X}_t - \eta_t \mathbf{O}_t. \quad (11)$$

Here, compared to the basic Muon (8),  $\mathbf{O}_t$  can be understood as the projection-based realization of the gradient-orthogonalized subspace RGE. See a full algorithmic description of ZO-Muon in Appendix C.

Furthermore, we provide a theoretical underpinning of the proposed ZO-Muon in (10)–(11) from a low-rank Muon perspective. As shown in (10), the RGE inside the `mSIGN` operator prior to GO corresponds to an approximation of the subspace-projected gradient  $\mathbf{P}^\top \nabla_{\mathbf{X}} f(\mathbf{X})$ , as given by (5) and the step ① in (4). Therefore, the FO interpretation of the ZO-Muon step (10) yields

$$\mathbf{O} = \mathbf{P} \text{msign}(\mathbf{P}^\top \mathbf{G}), \quad \mathbf{G} = \nabla_{\mathbf{X}} f(\mathbf{X}), \quad (12)$$

where, for notational simplicity, we omit the iteration index  $t$ . Clearly, in the absence of the projection  $\mathbf{P} \in \mathbb{R}^{m \times r}$ , the step (12) reduces to the standard GO update in Muon (8). Since  $r \ll \min\{m, n\}$ , the GO step (12) is applied to the low-rank matrix  $\mathbf{P}^\top \mathbf{G}$ , rather than to the full gradient  $\mathbf{G} \in \mathbb{R}^{m \times n}$ . Proposition 1 below shows *when* the GO step (12) becomes equivalent to the original GO step (9).

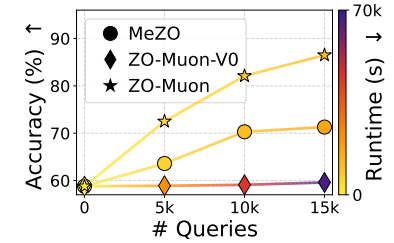


Figure 5: Demonstration of the ineffectiveness of ZO-Muon-V0 vs. MeZO and the effectiveness of ZO-Muon through fine-tuning OPT-13B on SST-2.

**Proposition 1** *If the projection is chosen as  $\mathbf{P} = \mathbf{U}_{[:,k]} \in \mathbb{R}^{m \times k}$ , obtained from the SVD of  $\mathbf{G}$  in (9), then the projection for gradient orthogonalization is lossless. That is,*

$$\mathbf{P} \text{msign}(\mathbf{P}^\top \mathbf{G}) = \text{msign}(\mathbf{G}). \quad (13)$$

**Proof:** See details in [Appendix D](#). □

Together w/ Prop. 1, our analysis shows that ZO-Muon (10) can be viewed as a ZO approximation of low-rank Muon (12). In the FO setting, it has been shown to outperform standard Muon in LLM pretraining (He et al., 2025).

**Design choices in ZO-Muon: Query number  $N_q$  and projection rank  $r$ .** First, we find that setting the query number  $N_q > 1$  is crucial for ZO-Muon, e.g.,  $N_q = 4$  works well in our experiments, indicating that the RGE (10) should be implemented in its multi-query form. Recall from (10) that in the absence of msign, the method reduces to Subspace RGE, yielding Subspace-MeZO as examined in Fig. 3. For both Subspace-MeZO and its full-space baseline MeZO (Malladi et al., 2023), the default choice is  $N_q = 1$ . This is due to the *multi-query paradox* (Lin et al., 2025): Although using multiple queries per iteration can reduce the variance of the gradient estimate, whether it improves optimization performance depends on how the queries are aggregated. In particular, simple averaging with  $N_q > 1$  can lead to diminishing returns (*i.e.*, the multi-query paradox) compared to using a single query per iteration.

However, unlike Subspace-MeZO, when  $N_q = 1$  is used in ZO-Muon, the GO step (10) reduces to  $\text{msign}(s\Psi) = \text{sign}(s)\text{msign}(\Psi)$ , where  $s = \frac{f(\mathbf{X} + \mu\mathbf{P}\Psi) - f(\mathbf{X})}{\mu}$  is the finite-difference scalar and  $s\Psi$  is the RGE. Here,  $\text{sign}(s)$  returns 1 or  $-1$  depending on the sign of  $s$ . In this case, even when the RGE magnitude  $s$  becomes small (towards convergence), the msign operation discards its scale and may amplify small noise by enforcing a spectrally isotropic update. Therefore, ZO-Muon benefits from using  $N_q > 1$ . In addition, it can effectively overcome the multi-query paradox compared to Subspace-MeZO (see [Appendix E](#) for empirical validation).

For the other key hyperparameter, the projection rank  $r$  that defines the subspace via  $\mathbf{P}$ , we find that ZO-Muon remains effective as long as it is set to a reasonably reduced dimension (e.g.,  $r \in \{64, 128\}$ ). This is roughly aligned with the effective rank of FO gradients shown in Fig. 3(a). To validate this, [Fig. 6](#) compares the performance of ZO-Muon with Subspace-MeZO under different values of  $r$  when fine-tuning OPT-1.3B on SST-2 and SQuAD. As shown in [Fig. 6\(a\)](#), ZO-Muon consistently outperforms Subspace-MeZO across all rank choices (indicating the usefulness of GO in ZO-Muon) and achieves the best performance with a moderate rank such as  $r = 64$ . Setting  $r$  too small or too large degrades the performance of ZO-Muon: A too-small  $r$  discards informative gradient components during projection, while an overly large  $r$  amplifies noisy directions after GO. This is further supported by [Fig. 6\(b\)](#), which shows that ZO-Muon converges slowly when  $r$  is too small, whereas using an overly large rank (e.g.,  $r = 256$ ) leads to instability and loss increase in the later stage of training, likely due to excessive gradient noise in ZO optimization.

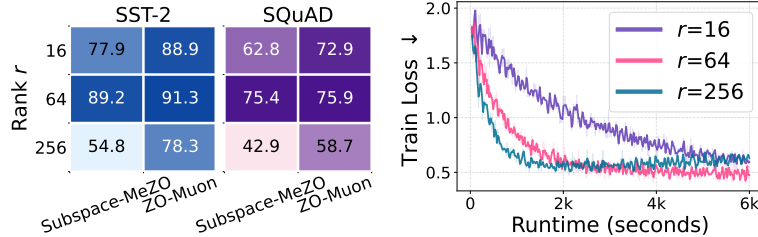


Figure 6: Comparison of ZO-Muon and Subspace-MeZO for fine-tuning OPT-1.3B on SST-2 and SQuAD with  $r \in \{16, 64, 256\}$ . (Left) Fine-tuning accuracy (shown by cell color and numeric value) for different  $r$ . ZO-Muon consistently outperforms Subspace-MeZO, with  $r = 64$  achieving the best performance. (Right) Training loss curves of ZO-Muon under different projection ranks for fine-tuning OPT-1.3B on SQuAD.

## 5 Experiments

### 5.1 Experiment setups

**Models and datasets.** We evaluate the performance of ZO optimization on fine-tuning tasks for both LLMs and ViTs. For LLMs, we primarily consider LLaMA3-8B (Grattafiori et al., 2024) and OPT-1.3B/13B (Zhang et al., 2022a) on the SuperGLUE benchmark (Wang et al., 2019). For ViTs, we fine-tune ViT-B/16 and ViT-L/16 (Dosovitskiy et al., 2021) on the CIFAR-10/100 datasets (Krizhevsky et al., 2009).

**Baselines and evaluations.** We compare the proposed ZO-Muon with the following stateful ZO optimization baselines, which were primarily developed for large-model fine-tuning. These include MeZO (Malladi et al., 2023), SparseMeZO

(S-MeZO) (Liu et al., 2025a), HiZOO (Zhao et al., 2025a), LOZO (Chen et al., 2025b), SubZero (Yu et al., 2025), and Subspace-MeZO developed in Sec. 3 prior to integration with Muon. We do not include other recent ZO optimization methods such as FZOO (Dang et al., 2025) and MUZO (Peng et al., 2025) in our comparison, as we were unable to find open-source and reproducible implementations for these approaches. In addition to ZO approaches, we also include FO baselines, Adam (Kingma, 2014) and LoRA (with Adam) (Hu et al., 2022).

**Implementation details.** For ZO-Muon, we perform a hyperparameter grid search over the projection rank  $r \in \{64, 128\}$  across all settings, following the rank selection rationale in Sec. 4. We also search over  $N_q \in \{4, 8, 16\}$ , consistent with our justification for using  $N_q > 1$  in Sec. 4. Empirically, we find that setting  $N_q = 16$  and  $r = 64$  for ViTs, and using  $N_q = 4$  with  $r \in \{64, 128\}$  for LLMs depending on the task, consistently yields strong performance. To ensure a fair comparison with other baselines, we scale the number of training steps inversely with  $N_q$ , so that ZO-Muon does not incur additional query or runtime overhead. The projection matrix  $\mathbf{P}$  is resampled via QR decomposition every 100 iterations (*i.e.*, lazily updated);

For the `msign` operation, we use the NS (Newton–Schulz) iteration unless otherwise specified. We set the training batch size to 16 for all LLM experiments, and to 64 and 256 for ViT fine-tuning on CIFAR-10 and CIFAR-100, respectively. The rationale for these choices is supported by the experimental results presented later.

Additional experiment setups, including settings of baselines, are detailed in Appendix F.

## 5.2 Experiment results

Table 1: ZO-Muon outperforms the ZO baselines by a non-negligible margin, demonstrated by fine-tuning LLMs (LlaMA3-8B and OPT-13B) on SuperGLUE benchmark and fine-tuning ViTs (ViT-B and ViT-L) on CIFAR datasets. FO methods (marked by  $\bullet$ ) include Adam and LoRA. The best ZO fine-tuning result for each task is highlighted in **bold**.

Method	LLM Fine-tuning						ViT Fine-tuning	
	SST-2	RTE	CB	BoolQ	WiC	SQuAD	CIFAR-10	CIFAR-100
	LlaMA3-8B						ViT-B	
• Adam	96.0	92.0	92.0	86.6	72.6	90.4	98.9	91.2
• LoRA	95.0	80.9	73.2	86.4	70.7	89.4	98.3	86.4
MeZO	92.7	74.4	<b>69.6</b>	76.7	57.8	86.7	93.5	64.5
S-MeZO	92.1	69.7	69.6	80.5	56.9	87.5	93.7	64.3
HiZOO	93.5	75.1	69.6	80.0	59.7	87.3	93.2	64.9
LOZO	92.5	66.8	<b>69.6</b>	79.4	55.8	<b>89.0</b>	93.2	61.8
SubZero	92.1	71.4	67.9	82.0	58.8	88.3	41.1*	7.3*
Subspace-MeZO	92.3	68.6	<b>69.6</b>	80.0	62.9	84.5	94.2	58.2
<b>ZO-Muon</b>	<b>94.3</b>	<b>81.2</b>	<b>69.6</b>	<b>82.9</b>	<b>65.2</b>	88.2	<b>94.9</b>	<b>72.6</b>
OPT-13B								
• Adam	95.3	80.9	94.6	83.5	66.3	89.5	98.8	91.7
• LoRA	94.8	78.3	69.6	80.2	64.3	88.0	98.8	90.6
MeZO	91.4	66.1	66.0	66.1	59.4	81.8	95.6	47.3
S-MeZO	90.4	63.5	69.6	66.4	58.8	80.8	96.9	56.3
HiZOO	92.1	69.3	69.6	67.6	59.4	82.1	96.3	46.6
LOZO	91.7	70.4	69.6	71.9	60.2	<b>84.9</b>	95.3	48.9
SubZero	92.1	71.8	<b>71.4</b>	70.8	60.8	84.5	41.2*	3.2*
Subspace-MeZO	91.7	70.7	<b>71.4</b>	68.1	<b>61.7</b>	83.5	97.0	64.7
<b>ZO-Muon</b>	<b>92.5</b>	<b>72.9</b>	<b>71.4</b>	<b>72.4</b>	<b>61.7</b>	84.5	<b>97.2</b>	<b>72.4</b>

\* SubZero underperforms despite extensive hyperparameter tuning, likely due to training instability caused by the double-projection RGE.

**ZO-Muon achieves superior ZO fine-tuning accuracy for both LLMs and ViTs.** In Tab. 1, we compare the LLM and ViT fine-tuning performance of ZO-Muon with FO and ZO baselines (listed by rows) on LlaMA3-8B and OPT-13B, as well as ViT-B and ViT-L, where each column corresponds to a fine-tuning task. As shown, ZO-Muon consistently improves fine-tuning accuracy over existing ZO baselines. In particular, for higher-complexity tasks such as RTE and WiC in LLM fine-tuning and CIFAR-100 in ViT fine-tuning, ZO-Muon achieves substantial gains, elevating ZO optimization to a new level, narrowing the gap to FO baselines. Notably, on ViT-L CIFAR-100 fine-tuning, ZO-Muon outperforms the second-best ZO method (Subspace-MeZO) by 7.7% and MeZO by 25.1% in accuracy. In addition, we observe that Subspace-MeZO consistently ranks among the top-performing ZO baselines, and that ZO-Muon further improves upon it. This indicates that subspace ZO and Muon’s GO (gradient orthogonalization) provide complementary benefits for improving overall ZO optimization.

Table 2: Efficiency comparison in terms of the number of optimization steps, number of queries, runtime, memory cost, GPU usage, and accuracy for fine-tuning OPT-13B on SST-2. Note that the total query budget is fixed to 40k for all ZO methods.

Method	Steps ↓	Queries ↓	Runtime ↓	Memory ↓	GPUs ↓	Accuracy ↑
Adam	625	625	10min	$4 \times 63.7$ GB	$4 \times$ A100	95.3
LoRA	625	625	6min	$2 \times 52.7$ GB	$2 \times$ A100	94.8
MeZO	20k	40k	3h 37min	28.2 GB	1 × A100	91.4
S-MeZO	20k	40k	6h 46min	30.1 GB	1 × A100	90.4
HiZOO	13.3k	40k	4h 46min	55.4 GB	1 × A100	92.1
LOZO	20k	40k	3h 19min	27.6 GB	1 × A100	91.7
SubZero	20k	40k	3h 23min	28.6 GB	1 × A100	92.1
Subspace-MeZO	20k	40k	3h 27min	28.6 GB	1 × A100	91.7
<b>ZO-Muon</b>	8k	40k	2h 33min	29.0 GB	1 × A100	92.5

**ZO-Muon delivers a strong efficiency profile over other ZO baselines.** In [Tab. 2](#), we compare the efficiency of ZO-Muon with ZO and FO baselines in terms of the number of optimization steps, number of queries, runtime, memory cost, and GPU usage for fine-tuning OPT-13B on SST-2, with the corresponding accuracy results reported in [Tab. 1](#). For a fair comparison, we fix the total query budget for gradient estimation during fine-tuning to 40k for all ZO methods. As we can see, ZO-Muon significantly reduces the number of ZO optimization steps and thereby yield the improved runtime efficiency compared to other ZO baselines. For example, ZO-Muon requires only 70.5% of MeZO’s runtime while outperforming it by 1.1% in fine-tuning accuracy. In addition, compared to FO approaches, ZO optimization does not offer a runtime advantage, but it significantly reduces memory cost and GPU requirements. This is the primary motivation for using ZO fine-tuning as a memory-efficient alternative to FO fine-tuning. We observe that ZO-Muon inherits this advantage and does not increase memory cost or GPU usage compared to other ZO baselines.

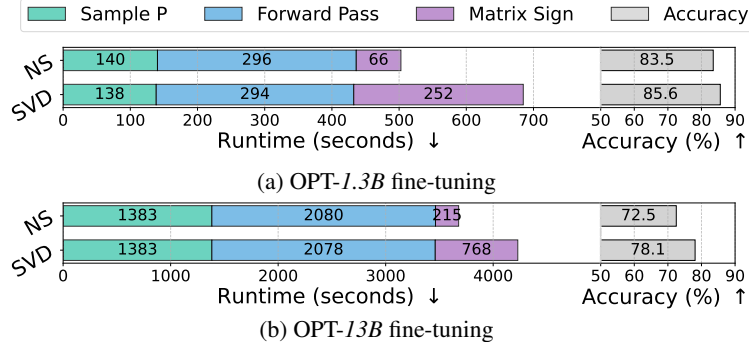


Figure 7: Runtime and accuracy comparison of ZO-Muon using NS and SVD for fine-tuning OPT-1.3B/13B on SST-2 under the same query budget (5,000).

**SVD vs. Newton–Schulz in ZO-Muon.** Thanks to the subspace projection in ZO-Muon (10), the msign operation, previously the main computational bottleneck in Muon, can now be computed via exact SVD as in (9), instead of using NS iterations (Jordan et al., 2024). Thus, [Fig. 7](#) compares the runtime and accuracy of ZO-Muon using NS (the default choice) vs. SVD when fine-tuning OPT-1.3B/13B on SST-2. The runtime is further decomposed into three components: sampling the projection matrix  $P$ , forward passes for ZO gradient estimation, and the msign computation. As shown, using SVD for exact msign computation indeed improves accuracy over the NS-based implementation. However, SVD incurs approximately 3× higher runtime than NS for the matrix-sign operation. This substantial efficiency gap is the primary reason we adopt NS in ZO-Muon.

**ZO-Muon does not rely on large batch sizes.** In ZO optimization, increasing the batch size reduces gradient-estimation variance but also raises memory usage, since GPU cost is dominated by forward passes. We therefore study ZO performance as a function of batch size. [Fig. 8](#) compares accuracy and GPU memory of ZO-Muon and baselines for ViT-B fine-tuning on CIFAR-100 under batch sizes 64, 128, and 256. While larger batches generally improve ZO accuracy, reducing the batch size from 256 to 64 causes a severe drop for baselines (*e.g.*, 22.2% for MeZO) but only a modest drop for ZO-Muon (6.2%). Notably, ZO-Muon with batch size 64 still outperforms MeZO with batch size 256. Together with [Fig. 8\(b\)](#), which shows the higher memory cost of larger batches, these results demonstrate that ZO-Muon is substantially more memory-efficient. The same advantage in resilience to batch size selection is observed for LLM fine-tuning, as shown in [Fig. A6](#).

**Additional results.** We report additional validations in [Appendix G](#). [Fig. A3](#) shows the fast convergence of ZO-Muon across multiple datasets, complementing [Fig. 1](#). [Tab. A2](#) reports results on Gemma2-2B (Team et al., 2024), where

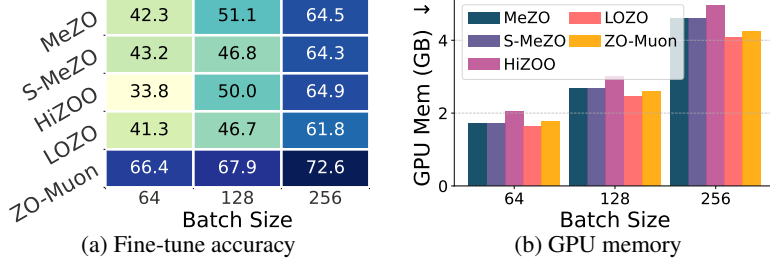


Figure 8: Accuracy and GPU memory comparison under varying batch sizes. ZO-Muon vs. baselines on ViT-B fine-tuning for CIFAR-100 with a fixed query budget.

ZO-Muon again consistently outperforms other ZO methods, in line with Tab. 1. We also study the resampling frequency of the projection matrix  $\mathbf{P}$  and show that lazy resampling stabilizes ZO training in Fig. A4, and we find random sampling  $\mathbf{P}$  both effective and efficient, shown in Tab. A3.

## 6 Conclusion

In this paper, we propose ZO-Muon, a novel ZO optimization method that bridges the gap between memory efficiency and convergence speed in deep model training. By combining subspace optimization with spectral gradient orthogonalization, ZO-Muon resolves the fundamental variance–efficiency tension in standard ZO methods. Extensive experiments on LLMs and ViTs show that ZO-Muon consistently outperforms state-of-the-art baselines in both performance and efficiency. Despite these gains, our work has limitations that point to future directions: we focus on parameter-efficient fine-tuning, and extending ZO-Muon to full pre-training of large-scale models remains open.

## Impact Statement

This work aims to advance zeroth-order (ZO) optimization for deep learning, with the goal of improving the accuracy and efficiency of fine-tuning large-scale neural networks without using backpropagation. By substantially reducing memory overhead and improving query efficiency, the proposed method (ZO-Muon) lowers the computational barrier for adapting large models, potentially enabling a broader community of researchers and practitioners with limited resources to work with foundation models. More broadly, reducing reliance on first-order gradients in model training and adaptation can contribute to lower energy consumption and more sustainable use of computational resources. At the same time, increased accessibility to powerful models may accelerate progress across a wide range of scientific and engineering applications. All experiments in this paper are conducted using publicly available models and datasets. The method itself is a general model training technique and does not introduce new capabilities that are inherently harmful. We do not foresee any immediate negative societal impacts directly resulting from this work.

## Acknowledgment

The work of Y. Lang, C. Wang, Y. Zhang, and S. Liu was supported in part by the National Science Foundation (NSF) CAREER Award IIS-2338068 and the Cisco Research Award. Z. Zhang was supported by NSF CCF-2419889.

## References

- J. Achiam, S. Adler, S. Agarwal, L. Ahmad, I. Akkaya, F. L. Aleman, D. Almeida, J. Altenschmidt, S. Altman, S. Anadkat *et al.*, “Gpt-4 technical report,” *arXiv preprint arXiv:2303.08774*, 2023.
- S. Zhang, S. Roller, N. Goyal, M. Artetxe, M. Chen, S. Chen, C. Dewan, M. Diab, X. Li, X. V. Lin *et al.*, “Opt: Open pre-trained transformer language models,” *arXiv preprint arXiv:2205.01068*, 2022.
- H. Touvron, L. Martin, K. Stone, P. Albert, A. Almahairi, Y. Babaei, N. Bashlykov, S. Batra, P. Bhargava, S. Bhosale *et al.*, “Llama 2: Open foundation and fine-tuned chat models,” *arXiv preprint arXiv:2307.09288*, 2023.
- S.-i. Amari, “Backpropagation and stochastic gradient descent method,” *Neurocomputing*, vol. 5, no. 4-5, pp. 185–196, 1993.
- D. P. Kingma, “Adam: A method for stochastic optimization,” *arXiv preprint arXiv:1412.6980*, 2014.

Y. Chen, Y. Zhang, Y. Liu, K. Yuan, and Z. Wen, “A memory efficient randomized subspace optimization method for training large language models,” in *Forty-second International Conference on Machine Learning*, 2025. [Online]. Available: <https://openreview.net/forum?id=XuCf87V8OF>

S. Liu, P.-Y. Chen, B. Kailkhura, G. Zhang, A. O. Hero III, and P. K. Varshney, “A primer on zeroth-order optimization in signal processing and machine learning: Principles, recent advances, and applications,” *IEEE Signal Processing Magazine*, vol. 37, no. 5, pp. 43–54, 2020.

J. C. Duchi, M. I. Jordan, M. J. Wainwright, and A. Wibisono, “Optimal rates for zero-order convex optimization: The power of two function evaluations,” *IEEE Transactions on Information Theory*, vol. 61, no. 5, pp. 2788–2806, 2015.

Y. Nesterov and V. Spokoiny, “Random gradient-free minimization of convex functions,” *Foundations of Computational Mathematics*, vol. 17, no. 2, pp. 527–566, 2017.

S. Malladi, T. Gao, E. Nichani, A. Damian, J. D. Lee, D. Chen, and S. Arora, “Fine-tuning language models with just forward passes,” in *Thirty-seventh Conference on Neural Information Processing Systems*, 2023. [Online]. Available: <https://openreview.net/forum?id=Vota6rFhBQ>

Y. Zhang, P. Li, J. Hong, J. Li, Y. Zhang, W. Zheng, P.-Y. Chen, J. D. Lee, W. Yin, M. Hong *et al.*, “Revisiting zeroth-order optimization for memory-efficient llm fine-tuning: A benchmark,” in *International Conference on Machine Learning*. PMLR, 2024, pp. 59 173–59 190.

Q. Tan, J. Liu, Z. Zhan, C. Ding, Y. Wang, X. Ma, J. Lee, J. Lu, and G. Yuan, “Harmony in divergence: Towards fast, accurate, and memory-efficient zeroth-order LLM fine-tuning,” in *The Thirty-ninth Annual Conference on Neural Information Processing Systems*, 2025. [Online]. Available: <https://openreview.net/forum?id=Rx6m16By6l>

Y. Liu, Z. Zhu, C. Gong, M. Cheng, C.-J. Hsieh, and Y. You, “Sparse meZO: Less parameters for better performance in zeroth-order LLM fine-tuning,” in *The Thirty-ninth Annual Conference on Neural Information Processing Systems*, 2025. [Online]. Available: <https://openreview.net/forum?id=Tjw0ACu3NL>

P.-Y. Chen, H. Zhang, Y. Sharma, J. Yi, and C.-J. Hsieh, “Zoo: Zeroth order optimization based black-box attacks to deep neural networks without training substitute models,” in *Proceedings of the 10th ACM workshop on artificial intelligence and security*, 2017, pp. 15–26.

A. Ilyas, L. Engstrom, A. Athalye, and J. Lin, “Black-box adversarial attacks with limited queries and information,” in *International conference on machine learning*. PMLR, 2018, pp. 2137–2146.

P. Zhao, S. Liu, P.-Y. Chen, N. Hoang, K. Xu, B. Kailkhura, and X. Lin, “On the design of black-box adversarial examples by leveraging gradient-free optimization and operator splitting method,” in *Proceedings of the IEEE/CVF International Conference on Computer Vision*, 2019, pp. 121–130.

A. Chen, Y. Zhang, J. Jia, J. Diffenderfer, J. Liu, K. Parasyris, Y. Zhang, Z. Zhang, B. Kailkhura, and S. Liu, “Deepzero: Scaling up zeroth-order optimization for deep model training,” *arXiv preprint arXiv:2310.02025*, 2023.

Y. Chen, Y. Zhang, L. Cao, K. Yuan, and Z. Wen, “Enhancing zeroth-order fine-tuning for language models with low-rank structures,” in *The Thirteenth International Conference on Learning Representations*, 2025. [Online]. Available: <https://openreview.net/forum?id=9BiVepgmWW>

Y. Zhao, S. Dang, H. Ye, G. Dai, Y. Qian, and I. Tsang, “Second-order fine-tuning without pain for LLMs: A hessian informed zeroth-order optimizer,” in *The Thirteenth International Conference on Learning Representations*, 2025. [Online]. Available: <https://openreview.net/forum?id=bEqI61iBue>

S. Liu, J. Chen, P.-Y. Chen, and A. Hero, “Zeroth-order online alternating direction method of multipliers: Convergence analysis and applications,” in *International Conference on Artificial Intelligence and Statistics*. PMLR, 2018, pp. 288–297.

S. Liu, B. Kailkhura, P.-Y. Chen, P. Ting, S. Chang, and L. Amini, “Zeroth-order stochastic variance reduction for nonconvex optimization,” *Advances in neural information processing systems*, vol. 31, 2018.

H. Zhao, S. Ding, C. Fang, and Z. Lin, “PaZO: Preconditioned accelerated zeroth-order optimization for fine-tuning LLMs,” in *The Thirty-ninth Annual Conference on Neural Information Processing Systems*, 2025. [Online]. Available: <https://openreview.net/forum?id=b2IU6QOOfo>

S. Ma and H. Huang, “Revisiting zeroth-order optimization: Minimum-variance two-point estimators and directionally aligned perturbations,” in *The Thirteenth International Conference on Learning Representations*, 2025.

W. Guo, J. Long, Y. Zeng, Z. Liu, X. Yang, Y. Ran, J. R. Gardner, O. Bastani, C. De Sa, X. Yu *et al.*, “Zeroth-order fine-tuning of llms with extreme sparsity,” *arXiv preprint arXiv:2406.02913*, 2024.

Z. Yu, P. Zhou, S. Wang, J. Li, M. Tian, and H. Huang, “Zeroth-order fine-tuning of llms in random subspaces,” in *Proceedings of the IEEE/CVF International Conference on Computer Vision*, 2025, pp. 4475–4485.

W. Lin, Q. Song, and H. Xu, “The multi-query paradox in zeroth-order optimization,” *arXiv preprint arXiv:2509.15552*, 2025.

S. Dang, Y. Guo, Y. Zhao, H. Ye, X. Zheng, G. Dai, and I. Tsang, “Fzoo: Fast zeroth-order optimizer for fine-tuning large language models towards adam-scale speed,” *arXiv preprint arXiv:2506.09034*, 2025.

K. Ji, Z. Wang, Y. Zhou, and Y. Liang, “Improved zeroth-order variance reduced algorithms and analysis for nonconvex optimization,” in *International conference on machine learning*. PMLR, 2019, pp. 3100–3109.

Y. Peng, Y. Liu, F. Wen, and X. Chen, “Muzo: Leveraging multiple queries and momentum for zeroth-order fine-tuning of large language models,” in *Proceedings of the 2025 Conference on Empirical Methods in Natural Language Processing*, 2025, pp. 8577–8595.

K. Jordan, Y. Jin, V. Boza, J. You, F. Cesista, L. Newhouse, and J. Bernstein, “Muon: An optimizer for hidden layers in neural networks,” 2024. [Online]. Available: <https://kellerjordan.github.io/posts/muon/>

J. Liu, J. Su, X. Yao, Z. Jiang, G. Lai, Y. Du, Y. Qin, W. Xu, E. Lu, J. Yan *et al.*, “Muon is scalable for llm training,” *arXiv preprint arXiv:2502.16982*, 2025.

S. Ghadimi and G. Lan, “Stochastic first-and zeroth-order methods for nonconvex stochastic programming,” *SIAM journal on optimization*, vol. 23, no. 4, pp. 2341–2368, 2013.

K. Balasubramanian and S. Ghadimi, “Zeroth-order nonconvex stochastic optimization: Handling constraints, high dimensionality, and saddle points,” *Foundations of Computational Mathematics*, vol. 22, no. 1, pp. 35–76, 2022.

C.-C. Tu, P. Ting, P.-Y. Chen, S. Liu, H. Zhang, J. Yi, C.-J. Hsieh, and S.-M. Cheng, “Autozoom: Autoencoder-based zeroth order optimization method for attacking black-box neural networks,” in *Proceedings of the AAAI conference on artificial intelligence*, vol. 33, no. 01, 2019, pp. 742–749.

X. Chen, S. Liu, K. Xu, X. Li, X. Lin, M. Hong, and D. Cox, “Zo-adamm: Zeroth-order adaptive momentum method for black-box optimization,” *Advances in neural information processing systems*, vol. 32, 2019.

M. Cheng, T. Le, P.-Y. Chen, H. Zhang, J. Yi, and C.-J. Hsieh, “Query-efficient hard-label black-box attack: An optimization-based approach,” in *International Conference on Learning Representations*, 2019. [Online]. Available: <https://openreview.net/forum?id=rJlk6iRqKX>

S. Liu, S. Lu, X. Chen, Y. Feng, K. Xu, A. Al-Dujaili, M. Hong, and U.-M. O’Reilly, “Min-max optimization without gradients: Convergence and applications to black-box evasion and poisoning attacks,” in *International conference on machine learning*. PMLR, 2020, pp. 6282–6293.

Y. Zhang, Y. Yao, J. Jia, J. Yi, M. Hong, S. Chang, and S. Liu, “How to robustify black-box ML models? a zeroth-order optimization perspective,” in *International Conference on Learning Representations*, 2022. [Online]. Available: [https://openreview.net/forum?id=W9G\\_ImpHlQd](https://openreview.net/forum?id=W9G_ImpHlQd)

T. Sun, Y. Shao, H. Qian, X. Huang, and X. Qiu, “Black-box tuning for language-model-as-a-service,” in *International Conference on Machine Learning*. PMLR, 2022, pp. 20 841–20 855.

W. Hu, Y. Shu, Z. Yu, Z. Wu, X. Lin, Z. Dai, S.-K. Ng, and B. K. H. Low, “Localized zeroth-order prompt optimization,” *Advances in Neural Information Processing Systems*, vol. 37, pp. 86 309–86 345, 2024.

H. Zhang, Z. Liu, B. Gu, and Y. Chang, “Leveraging first and zeroth-order gradient to address imbalanced black-box prompt tuning via minimax optimization,” in *Proceedings of the AAAI Conference on Artificial Intelligence*, vol. 39, no. 21, 2025, pp. 22 407–22 415.

J. Gu, C. Feng, Z. Zhao, Z. Ying, R. T. Chen, and D. Z. Pan, “Efficient on-chip learning for optical neural networks through power-aware sparse zeroth-order optimization,” in *Proceedings of the AAAI conference on artificial intelligence*, vol. 35, no. 9, 2021, pp. 7583–7591.

P. Zhang, Y. Liu, Y. Zhou, X. Wei, and M. Chen, “When foresight pruning meets zeroth-order optimization: Efficient federated learning for low-memory devices,” *Journal of Systems Architecture*, vol. 168, p. 103526, 2025.

Q. Tan, S.-E. Chang, R. Xia, H. Ji, C. Yang, C. Zhang, J. Liu, Z. Zhan, Z. Fang, Z. Zou *et al.*, “Perturbation-efficient zeroth-order optimization for hardware-friendly on-device training,” in *2025 IEEE/ACM International Conference On Computer Aided Design (ICCAD)*. IEEE, 2025, pp. 1–9.

P. Kaushik, S. Chaudhari, A. Vaidya, R. Chellappa, and A. Yuille, “The universal weight subspace hypothesis,” *arXiv preprint arXiv:2512.05117*, 2025.

A. Aghajanyan, S. Gupta, and L. Zettlemoyer, “Intrinsic dimensionality explains the effectiveness of language model fine-tuning,” in *Proceedings of the 59th annual meeting of the association for computational linguistics and the 11th international joint conference on natural language processing (volume 1: long papers)*, 2021, pp. 7319–7328.

E. J. Hu, Y. Shen, P. Wallis, Z. Allen-Zhu, Y. Li, S. Wang, L. Wang, W. Chen *et al.*, “Lora: Low-rank adaptation of large language models.” *ICLR*, vol. 1, no. 2, p. 3, 2022.

J. Zhao, Z. Zhang, B. Chen, Z. Wang, A. Anandkumar, and Y. Tian, “Galore: Memory-efficient llm training by gradient low-rank projection,” *arXiv preprint arXiv:2403.03507*, 2024.

Y. Hao, Y. Cao, and L. Mou, “Flora: Low-rank adapters are secretly gradient compressors,” in *Forty-first International Conference on Machine Learning*, 2024. [Online]. Available: <https://openreview.net/forum?id=uubBZKM99Y>

T. Dettmers, A. Pagnoni, A. Holtzman, and L. Zettlemoyer, “Qlora: Efficient finetuning of quantized llms,” *Advances in neural information processing systems*, vol. 36, pp. 10 088–10 115, 2023.

H. Wang, Y. Li, S. Wang, G. Chen, and Y. Chen, “Milora: Harnessing minor singular components for parameter-efficient llm finetuning,” in *Proceedings of the 2025 Conference of the Nations of the Americas Chapter of the Association for Computational Linguistics: Human Language Technologies (Volume 1: Long Papers)*, 2025, pp. 4823–4836.

K. Lion, L. Zhang, B. Li, and N. He, “PoLAR: Polar-decomposed low-rank adapter representation,” in *The Thirty-ninth Annual Conference on Neural Information Processing Systems*, 2025. [Online]. Available: <https://openreview.net/forum?id=jDxFD45kkc>

Y. He, P. Li, Y. Hu, C. Chen, and K. Yuan, “Subspace optimization for large language models with convergence guarantees,” *arXiv preprint arXiv:2410.11289*, 2024.

K. Liang, B. Liu, L. Chen, and Q. Liu, “Memory-efficient llm training with online subspace descent,” *Advances in Neural Information Processing Systems*, vol. 37, pp. 64 412–64 432, 2024.

H. Zhang, J. Yin, G. Wang, Z. Liu, T. Zhang, A. Shrivastava, L. Yang, and V. Braverman, “I3s: Importance sampling subspace selection for low-rank optimization in llm pretraining,” *arXiv preprint arXiv:2502.05790*, 2025.

Y. Refael, G. Smorodinsky, T. Tirer, and O. Lindenbaum, “SUMO: Subspace-aware moment-orthogonalization for accelerating memory-efficient LLM training,” in *The Thirty-ninth Annual Conference on Neural Information Processing Systems*, 2025. [Online]. Available: <https://openreview.net/forum?id=DIjRvEKOeG>

D. Kozak, C. Molinari, L. Rosasco, L. Tenorio, and S. Villa, “Zeroth-order optimization with orthogonal random directions,” *Mathematical Programming*, vol. 199, no. 1, pp. 1179–1219, 2023.

R. Nozawa, P.-L. Poirion, and A. Takeda, “Zeroth-order random subspace algorithm for non-smooth convex optimization,” *Journal of Optimization Theory and Applications*, vol. 204, no. 3, p. 53, 2025.

C. Ma, W. Gong, M. Scetbon, and E. Meeds, “SWAN: SGD with normalization and whitening enables stateless LLM training,” in *Forty-second International Conference on Machine Learning*, 2025. [Online]. Available: <https://openreview.net/forum?id=CQZXGmw5vO>

A. Riabinin, E. Shulgin, K. Gruntkowska, and P. Richtárik, “Gluon: Making muon & scion great again!(bridging theory and practice of lmo-based optimizers for llms),” *arXiv preprint arXiv:2505.13416*, 2025.

A. Khaled, K. Ozkara, T. Yu, M. Hong, and Y. Park, “Muonbp: Faster muon via block-periodic orthogonalization,” *arXiv preprint arXiv:2510.16981*, 2025.

C. He, Z. Deng, and Z. Lu, “Low-rank orthogonalization for large-scale matrix optimization with applications to foundation model training,” *arXiv preprint arXiv:2509.11983*, 2025.

K. Ahn, B. Xu, N. Abreu, Y. Fan, G. Magakyan, P. Sharma, Z. Zhan, and J. Langford, “Dion: Distributed orthonormalized updates,” *arXiv preprint arXiv:2504.05295*, 2025.

N. Amsel, D. Persson, C. Musco, and R. M. Gower, “The polar express: Optimal matrix sign methods and their application to the muon algorithm,” *arXiv preprint arXiv:2505.16932*, 2025.

J. Bernstein and L. Newhouse, “Old optimizer, new norm: An anthology,” in *OPT 2024: Optimization for Machine Learning*, 2024. [Online]. Available: <https://openreview.net/forum?id=ux18f5nOpD>

E. Petrov, G. Evseev, A. Antonov, A. Veprikov, N. Bushkov, S. Moiseev, and A. Beznosikov, “Leveraging coordinate momentum in signsqd and muon: Memory-optimized zero-order,” *arXiv preprint arXiv:2506.04430*, 2025.

A. Grattafiori, A. Dubey, A. Jauhri, A. Pandey, A. Kadian, A. Al-Dahle, A. Letman, A. Mathur, A. Schelten, A. Vaughan *et al.*, “The llama 3 herd of models,” *arXiv preprint arXiv:2407.21783*, 2024.

A. Wang, Y. Pruksachatkun, N. Nangia, A. Singh, J. Michael, F. Hill, O. Levy, and S. Bowman, “Super glue: A stickier benchmark for general-purpose language understanding systems,” *Advances in neural information processing systems*, vol. 32, 2019.

A. Dosovitskiy, L. Beyer, A. Kolesnikov, D. Weissenborn, X. Zhai, T. Unterthiner, M. Dehghani, M. Minderer, G. Heigold, S. Gelly, J. Uszkoreit, and N. Houlsby, “An image is worth 16x16 words: Transformers for image recognition at scale,” in *International Conference on Learning Representations*, 2021. [Online]. Available: <https://openreview.net/forum?id=YicbFdNTTy>

A. Krizhevsky, G. Hinton *et al.*, “Learning multiple layers of features from tiny images,” 2009.

G. Team, M. Riviere, S. Pathak, P. G. Sessa, C. Hardin, S. Bhupatiraju, L. Hussenot, T. Mesnard, B. Shahriari, A. Ramé *et al.*, “Gemma 2: Improving open language models at a practical size,” *arXiv preprint arXiv:2408.00118*, 2024.

R. Socher, A. Perelygin, J. Wu, J. Chuang, C. D. Manning, A. Y. Ng, and C. Potts, “Recursive deep models for semantic compositionality over a sentiment treebank,” in *Proceedings of the 2013 conference on empirical methods in natural language processing*, 2013, pp. 1631–1642.

I. Dagan, O. Glickman, and B. Magnini, “The pascal recognising textual entailment challenge,” in *Machine learning challenges workshop*. Springer, 2005, pp. 177–190.

M.-C. De Marneffe, M. Simons, and J. Tonhauser, “The commitmentbank: Investigating projection in naturally occurring discourse,” in *proceedings of Sinn und Bedeutung*, vol. 23, no. 2, 2019, pp. 107–124.

C. Clark, K. Lee, M.-W. Chang, T. Kwiatkowski, M. Collins, and K. Toutanova, “Boolq: Exploring the surprising difficulty of natural yes/no questions,” in *Proceedings of the 2019 Conference of the North American Chapter of the Association for Computational Linguistics: Human Language Technologies, Volume 1 (Long and Short Papers)*, 2019, pp. 2924–2936.

M. T. Pilehvar and J. Camacho-Collados, “Wic: the word-in-context dataset for evaluating context-sensitive meaning representations,” in *Proceedings of the 2019 conference of the North American chapter of the association for computational linguistics: Human language technologies, volume 1 (Long and short papers)*, 2019, pp. 1267–1273.

P. Rajpurkar, J. Zhang, K. Lopyrev, and P. Liang, “Squad: 100,000+ questions for machine comprehension of text,” in *Proceedings of the 2016 Conference on Empirical Methods in Natural Language Processing*, 2016, pp. 2383–2392.

N. Halko, P.-G. Martinsson, and J. A. Tropp, “Finding structure with randomness: Probabilistic algorithms for constructing approximate matrix decompositions,” *SIAM review*, vol. 53, no. 2, pp. 217–288, 2011.

Y. Refael, J. Svirsky, B. Shustein, W. Huleihel, and O. Lindenbaum, “Adarankgrad: Adaptive gradient rank and moments for memory-efficient LLMs training and fine-tuning,” in *The Thirteenth International Conference on Learning Representations*, 2025. [Online]. Available: <https://openreview.net/forum?id=LvNROciCne>

## Appendix

### A Intrinsic Rank Measurement

To estimate the intrinsic dimensionality of the gradients, we perform Singular Value Decomposition (SVD) on the gradient matrix  $\mathbf{G}$ . Let  $\{\sigma_i\}_{i=1}^n$  denote the singular values of  $\mathbf{G}$  sorted in descending order. We determine the effective rank by identifying the number of principal components  $k$  required to capture 99.99% of the gradient energy. This relationship is formulated as finding the cutoff  $k$  satisfying:  $\mathcal{E}(k) = \frac{\sum_{i=1}^k \sigma_i^2}{\sum_{i=1}^n \sigma_i^2} \geq 0.9999$ .

### B Ineffectiveness of Full Space Gradient Orthogonalization

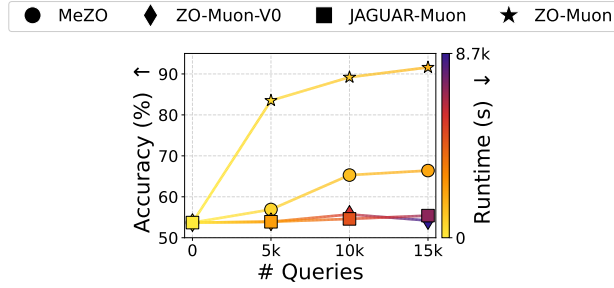


Figure A1: Fine-tune accuracy and runtime of full space gradient orthogonalization methods JAGUAR-Muon and ZO-Muon-V0 compared to MeZO and ZO-Muon, demonstrated by fine-tuning OPT-1.3B on SST-2.

Complementary to **Fig. 5**, we additionally validate the *ineffectiveness* of full space ZO gradient orthogonalization by fine-tuning OPT-1.3B on SST-2, shown in **Fig. A1**. With the same query number, ZO-Muon-V0 and JAGUAR-Muon (Petrov et al., 2025) does not outperform MeZO in fine-tune accuracy. Additionally, they consume more runtime compared to MeZO. In contrast, the *subspace* gradient orthogonalization ZO-Muon outperforms the above methods in accuracy and does not sacrifice runtime efficiency.

### C ZO-Muon Algorithm

**Algorithm 1** details our proposed ZO-Muon method. ZO-Muon treats parameters as matrices and optimizes layer-wise matrices  $\{\mathbf{X}_l\}$  where  $l$  represents each layer. First, the projection matrices  $\{\mathbf{P}_l\}$  are lazily sampled every interval  $v$ , corresponding to “*subspace sampling*”. Second, we perform *Subspace-RGE* following (5), making  $N_q > 1$  queries and performing a forward-difference estimate, and average the subspace ZO estimates. Finally, shown in “*full-space weight update*”, we follow (11) to orthogonalize the subspace gradient and project them back to full-space for model update.

---

#### Algorithm 1 ZO-Muon

---

```

Input: Parameters  $\mathbf{X} = \{\mathbf{X}_l\}$ , (where  $\mathbf{X}_l \in \mathbb{R}^{m_l \times n_l}$ ), loss function  $f(\mathbf{X})$ , projection matrices  $\mathbf{P} = \{\mathbf{P}_l\}$ , learning rate  $\eta$ , perturbation scale  $\mu$ , rank parameter  $r$ , query number  $N_q$ , projection matrix resample interval  $v$ , train steps  $T$ .
// Initialize Projection Matrices
Sample column-orthogonal projection matrices  $\{\mathbf{P}_l\}$  via QR decomposition.
for  $t = 0, \dots, T - 1$  do
  // 1. Subspace Sampling (Periodic Update)
  if  $t > 0$  and  $t \pmod{v} = 0$  then
    Resample  $\{\mathbf{P}_l\}$  via QR decomposition.
  end if
  // 2. Subspace-RGE
  Compute subspace ZO gradient estimate via (5) with  $N_q > 1$ .
  // 3. Full-space weight update
  Perform subspace gradient orthogonalization, then project back to full space via (10).
  Update model parameters via (11).
end for
Return  $\mathbf{X}$  ;

```

---

## D Proof of Proposition 1

**Proof:** With  $\text{msign}(\mathbf{G}) = \mathbf{G}(\mathbf{G}^\top \mathbf{G})^{-\frac{1}{2}}$  and using  $\mathbf{P}^\top \mathbf{P} = \mathbf{I}$ , we obtain

$$\begin{aligned} \mathbf{P} \text{msign}(\mathbf{P}^\top \mathbf{G}) &= \mathbf{P} \mathbf{P}^\top \mathbf{G} ((\mathbf{P}^\top \mathbf{G})^\top (\mathbf{P}^\top \mathbf{G}))^{-1/2} \\ &= \mathbf{P} \mathbf{P}^\top \mathbf{G} (\mathbf{G}^\top \mathbf{P} \mathbf{P}^\top \mathbf{G})^{-1/2}. \end{aligned} \quad (\text{A1})$$

Next, the SVD of  $\mathbf{G}$  yields

$$\mathbf{G} = \mathbf{U}_{[:,k]} \text{diag}(\boldsymbol{\sigma}) \mathbf{V}_{[:,k]}^\top,$$

where  $\text{diag}(\boldsymbol{\sigma}) \in \mathbb{R}^{k \times k}$  is the diagonal matrix containing the nonzero singular values of  $\mathbf{G}$ , and  $k = \text{rank}(\mathbf{G})$ .

Since  $\mathbf{P} = \mathbf{U}_{[:,k]}$  and  $\mathbf{P}^\top \mathbf{P} = \mathbf{I}$ , we have

$$\begin{aligned} \mathbf{P} \mathbf{P}^\top \mathbf{G} &= \mathbf{U}_{[:,k]} \mathbf{U}_{[:,k]}^\top \mathbf{U}_{[:,k]} \text{diag}(\boldsymbol{\sigma}) \mathbf{V}_{[:,k]}^\top \\ &= \mathbf{U}_{[:,k]} \text{diag}(\boldsymbol{\sigma}) \mathbf{V}_{[:,k]}^\top \\ &= \mathbf{G}. \end{aligned} \quad (\text{A2})$$

That is,  $\mathbf{P} \mathbf{P}^\top$  acts as the identity on the column space of  $\mathbf{G}$ . Substituting (A2) into (A1), we finally obtain  $\mathbf{P} \text{msign}(\mathbf{P}^\top \mathbf{G}) = \text{msign}(\mathbf{G})$ . This completes the proof.

## E Hyperparameter Study on $N_q$ in ZO-Muon

In Fig. A2, we compare ZO-Muon with Subspace-MeZO under different query number  $N_q$ , plotting performance against the total number of queries used during training. Shown in Fig. A2(a), there exists a multi-query paradox: Subspace-MeZO with  $N_q > 1$  performs worse than  $N_q = 1$ . On the contrary, ZO-Muon does not suffer from this issue (*i.e.*, additional queries do not lead to diminishing optimization returns). Moreover, as shown in Fig. A2(b), although ZO-Muon uses  $N_q = 4$ , this does not hurt query efficiency in practice compared to Subspace MeZO with  $N_q = 1$ , since ZO-Muon converges in significantly fewer iterations.

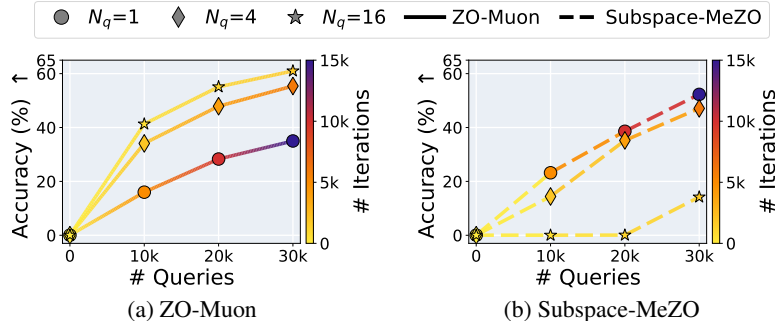


Figure A2: Fine-tuning accuracy vs. query cost for (a) ZO-Muon and (b) Subspace-MeZO when fine-tuning ViT-B on CIFAR-100, with marker color indicating the used iteration number. The per-iteration query budget is set to  $N_q \in \{1, 4, 16\}$ . (a) ZO-Muon benefits from increasing  $N_q$ , with a notable performance gain when moving from  $N_q = 1$  to  $N_q = 4$ . (b) Under the same setting, Subspace-MeZO exhibits a multi-query paradox, where performance degrades when  $N_q > 1$ .

## F Detailed Experiment Setups

**Models and datasets.** For LLM experiments, we evaluate Gemma2-2B (Team et al., 2024), LLaMA3-8B (Grattafiori et al., 2024) and OPT-13B (Zhang et al., 2022a) on the SuperGLUE benchmark (Wang et al., 2019), including the tasks SST-2 (Socher et al., 2013), RTE (Dagan et al., 2005), CB (De Marneffe et al., 2019), BoolQ (Clark et al., 2019), WiC (Pilehvar and Camacho-Collados, 2019) and SQuAD (Rajpurkar et al., 2016). Following previous literature (Malladi et al., 2023; Chen et al., 2025b; Zhao et al., 2025a; Yu et al., 2025), we randomly sample 1,000 train samples and 1,000 test samples. We adopt the same prompts as MeZO (Malladi et al., 2023).

For ViT experiments, we evaluate ViT-B/16 and ViT-L/16 (Dosovitskiy et al., 2021) fine-tuned on the CIFAR datasets (Krizhevsky et al., 2009). Data processing and evaluations are based on the well-established ViT pytorch code base<sup>1</sup>.

<sup>1</sup><https://github.com/jeonsworld/ViT-pytorch>

**Implementation details.** Our ZO-Muon, as well as baselines LOZO and SubZero treat model parameters as *matrices* instead of vectors. Following Muon (Jordan et al., 2024), we flatten the last three dimensions of 4D convolutional parameters and treat them as 2D matrices for optimization. Vector parameters, as well as the input and output layers, are optimized with MeZO.

**Hyperparameters.** We adopt hyperparameter settings consistent with existing literature to ensure rigorous benchmarking. For LLMs, we use a batch size of 16 and train for 20,000 steps, utilizing a constant learning rate without weight decay (Malladi et al., 2023; Chen et al., 2025b; Yu et al., 2025). The perturbation step size is fixed at  $\mu = 10^{-3}$  based on its demonstrated robustness across tasks (Malladi et al., 2023; Chen et al., 2025b). For ViT experiments, we set the batch size to 64 (CIFAR-10) and 256 (CIFAR-100). The necessity for increased batch sizes on CIFAR-100 is demonstrated in Fig. 8 and Sec. 5. We also fix the perturbation stepsize  $\mu = 10^{-3}$ . For algorithmic hyperparameters (e.g., sparsity for S-MeZO; rank  $r$  and interval  $v$  for subspace-based methods like LOZO and SubZero), we strictly follow the original baseline implementations. For LoRA, we follow previous works (Malladi et al., 2023; Chen et al., 2025b) and set rank  $r = 8$  and the scaling factor  $\alpha = 16$ . Detailed settings for both ZO and FO methods are listed in Tab. A1.

**Computing resources.** Experiments are primarily conducted on A6000 GPUs with 48GB memory. Runtime and GPU consumption evaluation in Tab. 2 are evaluated on A100 GPUs with 100GB memory since A6000 does not have enough memory for OPT-13B full Adam fine-tuning under our setting.

Table A1: Hyperparameter settings of ZO and FO methods used for fine-tuning LLMs and ViTs.

Methods	Hyperparameters	Values	
		LLM	ViT
MeZO	Learning rate	{1e - 7, 1e - 6} or {1e - 7, 5e - 7, 1e - 6} for SQuAD	{1e - 5, 1e - 4}
	Train steps	20k	20k
S-MeZO	Learning rate	{1e - 7, 1e - 6} or {1e - 7, 5e - 7, 1e - 6} for SQuAD	{1e - 5, 1e - 4}
	Sparsity	0.8	0.8
	Train steps	20k	20k
HiZOO	Learning rate	{1e - 7, 1e - 6} or {1e - 7, 5e - 7, 1e - 6} for SQuAD	{1e - 5, 1e - 4}
	Train steps	20k	20k
LOZO	Learning rate	{1e - 7, 1e - 6}	{1e - 5, 1e - 4}
	Rank ( $r$ )	{2, 4, 8}	{2, 4, 8}
	Interval ( $v$ )	100	100
	Train steps	20k	20k
SubZero	Learning rate	{1e - 7, 1e - 6}	{1e - 5, 1e - 4}
	Rank ( $r$ )	{24, 48}	{24, 48}
	Interval ( $v$ )	1000	1000
	Train steps	20k	20k
Subspace-MeZO	Learning rate	1e - 5	{1e - 5, 1e - 4}
	Rank ( $r$ )	{64, 128}	{64, 128}
	Interval ( $v$ )	100	100
	Train steps	20k	20k
ZO-Muon	Learning rate	1e - 2	1e - 2
	Rank ( $r$ )	{64, 128}	{64, 128}
	Interval ( $v$ )	100	100
	Train steps ( $N_q = 4$ )	8k	10k
	Train steps ( $N_q = 8$ )	4k	2k
	Train steps ( $N_q = 16$ )	-	2k
	Learning rate	{5e - 6, 1e - 5}	{1e - 3, 5e - 3}
Adam	Epochs	10	10
LoRA	Learning rate	{5e - 6, 1e - 5}	{1e - 3, 5e - 3}
	Epochs	10	10
	Rank ( $r$ )	8	8
	Alpha ( $\alpha$ )	16	16

## G Additional Experiment Results

**Loss curves of LLM fine-tuning.** Complementary to Fig. 1, Fig. A3 shows the training loss curves of ZO-Muon and representative baselines (MeZO and LOZO) for OPT-13B fine-tuning on four downstream tasks. Note that each method

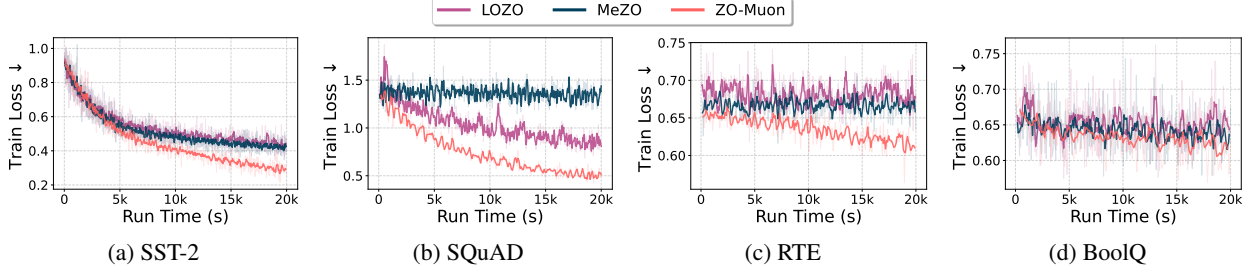


Figure A3: ZO-Muon achieves faster convergence rate compared to MeZO and LOZO, demonstrated through fine-tuning OPT-13B on SST-2, SQuAD, RTE and BoolQ.

is plotted using its best hyperparameter setting from the search grid (see Appendix F). Across all four tasks, ZO-Muon achieves the fastest convergence among the baselines.

**Gemma2-2B results.** **Tab. A2** presents fine-tuning results on Gemma2-2B. Consistent with Sec. 5.2, ZO-Muon achieves the best overall ZO performance and comes closest to FO methods. Notably, it improves over MeZO by 10.2% on RTE and 8.5% on BoolQ.

Table A2: Performance of ZO-Muon and baselines on Gemma2-2B under the same settings as Tab.1.

Method	Gemma2-2B Fine-tuning					
	SST-2	RTE	CB	BoolQ	WiC	SQuAD
• Adam	94.0	84.0	84.0	90.0	72.0	89.4
• LoRA	91.6	57.8	55.4	75.2	56.1	86.9
MeZO	91.7	53.0	60.7	66.1	57.1	74.1
S-MeZO	92.7	53.8	53.6	63.9	55.8	76.1
HiZOO	92.1	53.1	60.7	66.6	55.2	73.4
LOZO	92.2	56.3	57.1	65.0	50.2	77.3
SubZero	91.7	56.7	<b>67.8</b>	63.5	58.3	72.1
<b>ZO-Muon</b>	<b>94.2</b>	<b>63.2</b>	64.3	<b>74.6</b>	<b>60.3</b>	<b>78.4</b>

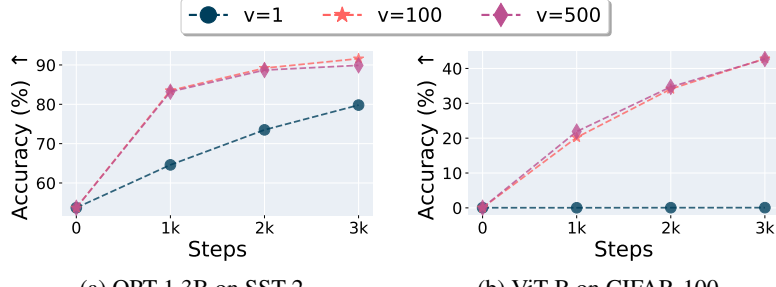


Figure A4: Performance of ZO-Muon with different projection matrix resampling interval  $v$ , demonstrated by (a) fine-tuning OPT-1.3B on SST-2 and (b) fine-tuning ViT-B on CIFAR-100.

**Projection matrix resampling interval** Recall that in ZO-Muon we *lazily* resample the subspace projection matrix  $\mathbf{P}$  every 100 steps (denoted by the resampling interval  $v = 100$ ). To validate this design choice, **Fig. A4** compares ZO-Muon with different resampling intervals  $v \in \{1, 100, 500\}$ . As shown, overly frequent resampling does not improve performance on either LLM or ViT fine-tuning. The case of  $v = 1$  consistently underperforms  $v = 100$ , while  $v = 500$  achieves performance comparable to  $v = 100$ . This is because frequent subspace switching (*i.e.*, resampling  $\mathbf{P}$ ) prevents the optimizer from sufficiently exploiting gradient information within a given subspace, leading to less stable training. Our lazy resampling strategy is also aligned with previous works on both FO training (Zhao et al., 2024; Refael et al., 2025a) and ZO training (Chen et al., 2025b; Yu et al., 2025)

**Projection matrix sampling strategies.** We present additional studies on sampling strategies for the projection matrices used in Subspace-MeZO and ZO-Muon, with results summarized in **Tab. A3**. Our default strategy, denoted as “Random,” constructs the projection matrix  $\mathbf{P} \in \mathbb{R}^{m \times r}$  via the QR decomposition of a Gaussian matrix. Alternatively,

the “*Sketching*” strategy applies Gaussian sketching (Halko et al., 2011) to past descending directions to capture informative subspace directions, a technique also utilized in first-order subspace training (He et al., 2025; Rafael et al., 2025b). Specifically, we maintain a momentum term  $\mathbf{M} \in \mathbb{R}^{m \times n}$  representing the moving average of past ZO gradients. The matrix  $\mathbf{P}$  is then derived by performing QR decomposition on  $\mathbf{MQ}$ , where  $\mathbf{Q} \in \mathbb{R}^{n \times r}$  is drawn from a Gaussian distribution. As shown in Tab. A3, Gaussian sketching does not yield notable performance gains over random sampling for either Subspace-MeZO or ZO-Muon, yet it increases GPU memory consumption, particularly for LLMs, due to the requirement of storing the momentum  $\mathbf{M}$ . In the ViT fine-tuning scenario, Gaussian sketching exhibits even worse accuracy, likely due to the cumulative bias introduced by Momentum as it accumulates past ZO gradient estimates rather than preciser FO gradients.

Table A3: Performance (evaluated by accuracy and F1) and GPU memory (short for “Mem”) of Subspace-MeZO and ZO-Muon with different projection matrix sampling strategies.

Method	Sampling Strategy	LlaMA3-8B Fine-tuning						ViT-B Fine-tuning			
		SST-2		RTE		SQuAD		CIFAR-10		CIFAR-100	
		Acc. (%) $\uparrow$	Mem (MiB) $\downarrow$	Acc. (%) $\uparrow$	Mem (MiB) $\downarrow$	F1 (%) $\uparrow$	Mem (MiB) $\downarrow$	Acc. (%) $\uparrow$	Mem (MiB) $\downarrow$	Acc. (%) $\uparrow$	Mem (MiB) $\downarrow$
Subspace-MeZO	Random Sketching	92.3	19058	68.6	28242	84.5	32102	94.2	1634	58.2	4086
	Sketching	92.3	34814	67.5	38874	87.2	44734	81.2	1898	29.1	4088
ZO-Muon	Random Sketching	94.3	19176	81.2	27224	88.2	30718	94.9	1686	72.6	4410
	Sketching	93.8	35268	78.3	44304	88.3	45248	95.3	1950	59.8	4412

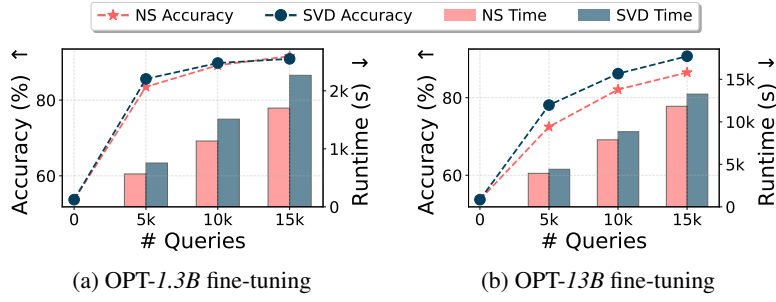


Figure A5: Fine-tuning accuracy and runtime of ZO-Muon using SVD vs. NS for gradient orthogonalization under the same query budget. Runtime is measured in seconds (s).

**SVD vs. NS in ZO-Muon.** Complementary to Fig. 7, Fig. A5 compares ZO-Muon using NS and SVD under different query budgets on OPT-1.3B and OPT-13B. Consistent with Sec. 5.2, SVD outperforms NS but incurs higher runtime. Moreover, the performance gap widens with model size: on OPT-1.3B (Fig. A5(a)), NS nearly matches SVD with 15k queries, whereas on OPT-13B (Fig. A5(b)) NS shows a larger gap. This aligns with the fact that the approximation error of NS increases with problem dimension (He et al., 2025).

**ZO-Muon does not rely on large batch sizes.** We extend the evaluation of ZO-Muon with decreased batch sizes in Fig. 8 to LLMs, evaluated by fine-tuning LlaMA3-8B on RTE, shown in Fig. A6. The results are aligned with the ViT results: ZO-Muon outperforms the baselines by a large margin with a decreased batch size. And ZO-Muon with a batch size of 4 outperforms S-MeZO and LOZO with a batch size of 16.

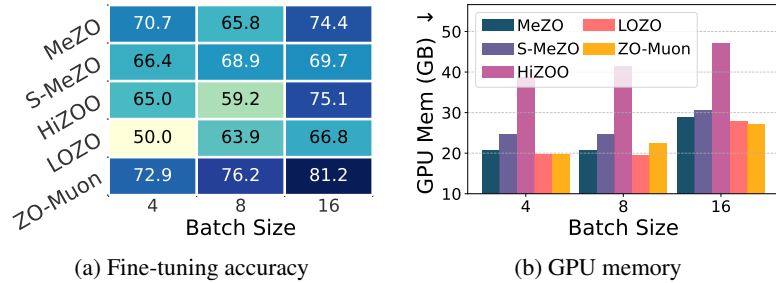


Figure A6: Fine-tuning accuracy and GPU memory comparison under varying batch sizes. ZO-Muon versus baselines on LlaMA3-8B fine-tuning for RTE with the same number of iterations.